Molecular Therapy
Original Article

PSCs Reveal PUFA-Provoked Mitochondrial Stress as a Central Node Potentiating RPE Degeneration in Bietti's Crystalline Dystrophy

Zhao Zhang,[1,8] Bin Yan,[2,5,7] Fei Gao,[1] Qing Li,[3] Xiaohong Meng,[4] Peikai Chen,[5] Lei Zhou,[5] Wen Deng,[5] Cheng Li,[1] Weiyi Xu,[5] Shuo Han,[1] Hong Feng,[1] Yaping Li,[6] Junhui Chen,[7] Zhengqin Yin,[4] Can Liao,[8] Hung-Fat Tse,[1] Aimin Xu,[1,9] and Qizhou Lian[1,8,9]

[1]Department of Medicine, LKS Faculty of Medicine, The University of Hong Kong, Hong Kong SAR, China; [2]Department of Computer Science, The University of Hong Kong, Hong Kong SAR, China; [3]Ophthalmology, Grantham Hospital, Hospital Authority, Hong Kong SAR, China; [4]Southwest Eye Hospital, Third Military Medical University, Chongqing 400038, China; [5]School of Biomedical Sciences, The University of Hong Kong, Hong Kong SAR, China; [6]Ophthalmology, The Second Hospital of Jilin University, Changchun 130022, China; [7]Intervention and Cell Therapy Center, Peking University Shenzhen Hospital, Shenzhen 518036, China; [8]Prenatal Diagnostic Centre and Cord Blood Bank, Guangzhou Women and Children's Medical Center, Guangzhou Medical University, Guangzhou 510623, China; [9]State Key Laboratory of Pharmaceutical Biotechnology, The University of Hong Kong, Hong Kong SAR, China

Bietti's crystalline dystrophy (BCD) is an incurable retinal disorder caused by the polypeptide 2 of cytochrome P450 family 4 subfamily V (*CYP4V2*) mutations. Patients with BCD present degeneration of retinal pigmented epithelial (RPE) cells and consequent blindness. The lack of appropriate disease models and patients' RPE cells limits our understanding of the pathological mechanism of RPE degeneration. In this study, using *CYP4V2* mutant pluripotent stem cells as disease models, we demonstrated that RPE cells with *CYP4V2* mutations presented a disrupted fatty acid homeostasis, which were characterized with excessive accumulation of poly-unsaturated fatty acid (PUFA), including arachidonic acid (AA) and eicosapentaenoic acid (EPA). The PUFA overload increased mitochondrial reactive oxygen species, impaired mitochondrial respiratory functions, and triggered mitochondrial stress-activated p53-independent apoptosis in *CYP4V2* mutant RPE cells. Restoration of the mutant *CYP4V2* using adeno-associated virus 2 (AAV2) can effectively reduce PUFA deposition, alleviate mitochondria oxidative stresses, and rescue RPE cell death in BCD RPE cells. Taken together, our results highlight a role of PUFA-induced mitochondrial damage as a central node to potentiate RPE degeneration in BCD patients. AAV2-mediated gene therapy may represent a feasible strategy for the treatment of BCD.

INTRODUCTION

Bietti's crystalline dystrophy (BCD) is a progressive chorioretinal disease first reported by Bettie[1] in 1937. Crystalline deposits appear in the fundus, and patients normally suffer night blindness in their 20s with gradual vision loss. Blindness develops during about 30 years due to chronic retinal degeneration.[2] The penetration frequency of BCD is rare in (around 1:67,000), but much more common in East Asians (more than 1:25,000).[2] Unfortunately, there is no effective treatment for BCD. Wilson et al.[3] first identified cholesterol-like crystals in biopsies of lymphocytes and fibroblasts from patients with BCD. This finding suggests that BCD is possible a lipid metabolic disorder. High-resolution optical coherence tomography (OCT) images showed that the crystals were deposited on the inner side of the retinal pigmented epithelium (RPE).[4,5] Li et al.[6] discovered that BCD was associated with gene mutations of *CYP4V2*, the polypeptide 2 of cytochrome P450 family 4 subfamily V. *CYP4V2* was highly expressed in the retina of human eyes, and it was thought to act by hydroxylating fatty acids in *in vitro* experiments.[7,8] Nonetheless, the systemic abnormality of fatty acid metabolism presented in patients with BCD could not be linked to genotypes of *CYP4V2* mutations, indicating the need for more detailed examination of fatty acid profiles in the retina.[9] It has been difficult to delineate how *CYP4V2* mutations change the lipid composition and the role of lipid crystals in retinal degeneration. A shortage of functional human retinal cells poses a challenge for pathological mechanism studies. Although the absence of *Cyp4v3* in a mouse model reproduced some clinical manifestations of BCD, the model did not truly recapitulate the retinal disorder of BCD in humans due to species differences in their retinal structure and physiology.[10] More research using a model relevant to human retinal disease is warranted.

Received 25 March 2020; accepted 21 July 2020;
https://doi.org/10.1016/j.ymthe.2020.07.024.

Correspondence: Qizhou Lian, MD, PhD, Department of Medicine, LKS Faculty of Medicine, The University of Hong Kong, Hong Kong SAR, China.
E-mail: qzlian@hku.hk
Correspondence: Aimin Xu, PhD, Department of Medicine, LKS Faculty of Medicine, The University of Hong Kong, Hong Kong SAR, China.
E-mail: amxu@hku.hk
Correspondence: Hung-Fat Tse, MD, PhD, Department of Medicine, LKS Faculty of Medicine, The University of Hong Kong, Hong Kong SAR, China.
E-mail: hftse@hku.hk

 © 2020 The Authors.
This is an open access article under the CC BY-NC-ND license (http://creativecommons.org/licenses/by-nc-nd/4.0/).

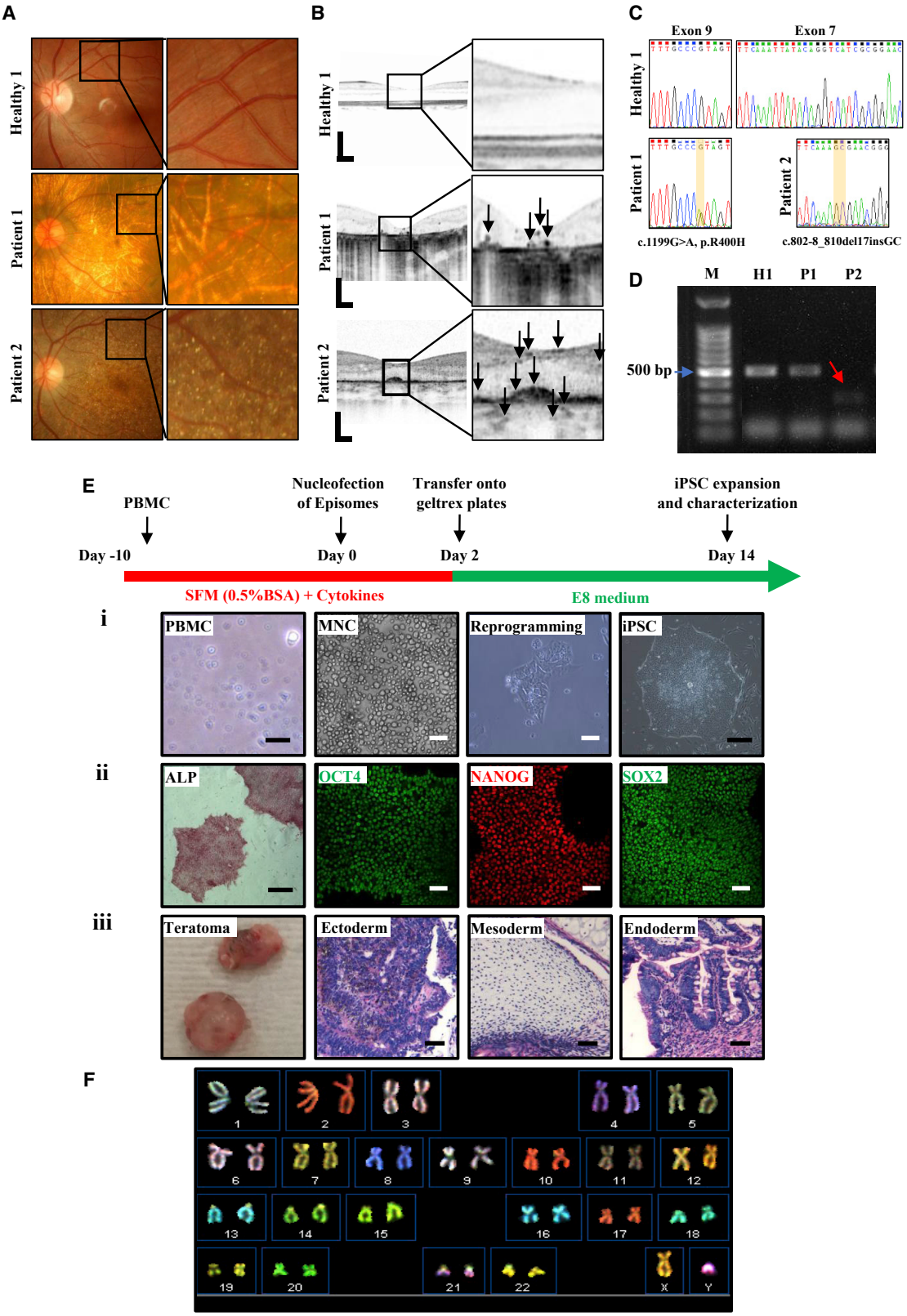

(legend on next page)

With the assistance of genome-editing techniques, such as transcription activator-like effector nuclease (TALEN) technology and CRISPR-Cas9, human pluripotent stem cells (PSCs) have recently provided an efficient means by which to model various human diseases and to examine effective treatments.[11] Human retinal cells, including RPE cells and photoreceptor cells, have also been successfully derived from human PSCs.[12,13] Use of parallel PSC control and a patient's induced PSCs (iPSCs) enables us to elucidate the pathological mechanisms of BCD and develop effective therapeutic strategies. Hata et al.[14] described several drugs that could rescue impaired autophagy flux and lysosomal dysfunction in BCD-iPSC-derived RPE cells by decreasing accumulated cholesterol. However, it was not clear what substance stimulated the autophagy in BCD-RPE cells. The cholesterol reduction could not halt the autophagy pathway, indicating that other mechanisms irrelevant to cholesterol-autophagy may play important roles in BCD-RPE degeneration. In addition, because of the blood-eye barrier, oral pharmacotherapy has little effect in retinal diseases. Until now, the profile and role of fatty acids in BCD-RPE have not been clearly established in human RPE cells. The human retina contains an abundance of fatty acids than other tissues, especially poly-unsaturated fatty acids. Some increased fatty acids in the serum of BCD patients as well as the fatty acid hydroxylation function of *CYP4V2* imply that BCD may be triggered by dysfunctional fatty acid metabolism as a result of *CYP4V2* mutations.[7–9,15] We hypothesize that *CYP4V2* mutation-provoked homeostasis disruption of fatty acid is a key role to induce RPE death in BCD. In this study, we generated *CYP4V2* mutant ($CYP4V2^{mt}$) RPE cells from patients' iPSCs and independent *CYP4V2* knockout PSC lines, and investigated their genotypes-phenotypes, whole-transcriptome sequencing, and fatty acid metabolism. Finally, we reported disrupted homeostasis of fatty acids in BCD-RPE; in particular, poly-unsaturated fatty acids (PUFAs), including arachidonic acid (AA) and eicosapentaenoic acid (EPA) were prominently increased. The PUFA-induced mitochondrial stress is a critical node that potentiates BCD-RPE degeneration. We further demonstrated that the adeno-associated virus 2 (AAV2)-mediated gene therapy could effectively rescue the *CYP4V2* mutation-induced BCD-RPE degeneration *in vitro*,[16,17] allowing us to explore AAV2-CYP4V2 gene therapy for BCD in the near future.

RESULTS

Generation of BCD Patient-Specific iPSCs

To establish the disease model, BCD patients and a healthy individual underwent careful evaluation of their clinical symptoms and genotype prior to reprogramming iPSCs. First, tiny crystalline deposits were identified on the fundus in BCD patients, but not in the healthy control (Figure 1A), evident on OCT imaging as small black points on the inner side of the RPE layer (Figure 1B). Sanger sequencing revealed a heterozygous point mutation (c.1199G>A, p.R400H) in patient 1 and one homozygous deletion (c.802-8_810del17insGC) in patient 2, both reported pathological mutations for BCD and not presented in the healthy control (Figure 1C).[18] Patient 1 was diagnosed with BCD by clinical manifestations, and mutation of *CYP4V2* in the coding region was identified in the first allele but not in the second allele. In some patients with BCD, pathological mutations of *CYP4V2* are often not presented in coding regions or are difficult to be identified in the second allele.[19–23] We thus further examined family co-segregation and copy number variants (CNVs) of *CYP4V2* in this patient. The pedigree showed a recessive inherited feature, but no CNV was found in all 11 exons of *CYP4V2* in this patient 1 (Figures S1A and S1B). In addition, family co-segregation disclosed that another older female was also diagnosed with BCD (Figure S1A). This older female presented similar clinical features and same mutation of *CYP4V2* (c.1199G>A, p.R400H) in an allele (data not shown). This indicated that other potential forms of *CYP4V2* mutations are not rare. i.e., in non-coding regions.[19–23] We also examined whether the gene mutations affected the alternative splicing of patients' *CYP4V2* in transcription and protein translation. For patient 2, the mRNA of *CYP4V2* lost the seventh exon, leading to the loss of α helix in its protein structure, while a shorter β sheet was predicted in patient 1's CYP4V2 protein because of the point mutation (Figures 1D and S1C).[24] Next, peripheral blood mononuclear cells (PBMCs) of three donors were collected for iPSC reprogramming using an integration-free episomal plasmid-based strategy (Figure 1E).[25,26] To characterize pluripotency of the iPSCs, alkaline phosphatase (ALP) staining was performed, and pluripotent markers, including OCT4, NANOG, and SOX2, were detected. Next, all iPSCs were subcutaneously transplanted into severe combined immunodeficiency (SCID) mice and formed teratomas. Ectoderm, mesoderm, and endoderm were identified using H&E staining. Karyotyping results indicated the normal chromosomes in healthy 1 iPSCs (Figure 1F). Characteristics of patients' iPSCs indicated that they were reprogrammed into the pluripotent stage with normal chromosomes as well (Figures S1D and S1E).

Fatty Acid Accumulations in $CYP4V2^{mt}$ PSCs

To reduce individual variations in the application of iPSCs for disease modeling, we also used well-documented commercial PSC lines (IMR90 and H9) with *CYP4V2* mutations.[11] Guide RNAs (gRNAs)

Figure 1. Diagnosis of BCD Batients and iPSC Reprogramming

(A) Fundus images taken from donors. The crystalline deposits appear as tiny bright yellow dots (arrow) in BCD patients. (B) OCT images show hyper-reflective crystalline deposits in whole layers of the retina and RPE (arrows) in BCD patients. Scale bars, 200 μm. (C) A heterozygous point mutation and a homozygous deletion were found in the *CYP4V2* of BCD patient 1 and patient 2, respectively. The mutations are highlighted with a yellow background. (D) Gel electrophoresis shows a shorter band of the *CYP4V2* transcripts in patient 2 because of the homozygous mutation. M, 100-bp ladder; H1, healthy 1-iPSC; P1, patient 1-iPSC; P2, patient 2-iPSC. (E) iPSC reprogramming and characterizations. (i) Isolated PBMCs were cultured in serum-free medium for 10 days to generate MNCs. After the nucleofection, MNCs were cultured continually in E8 medium until iPSC colonies emerged. (ii) ALP assay (red dye) and markers (OCT4, NANOG, and SOX2) for iPSCs in immunostaining. (iii) Teratoma formation and H&E staining: endoderm (intestinal epithelium-like), mesoderm (cartilage-like) and ectoderm (neural rosette-like) (healthy 1-iPSC). Scale bars, 15 μm for PBMCs, 200 μm for iPSCs and ALP, and 50 μm for others. (F) Karyotypes of healthy 1-iPSC. No abnormal chromosome was found.

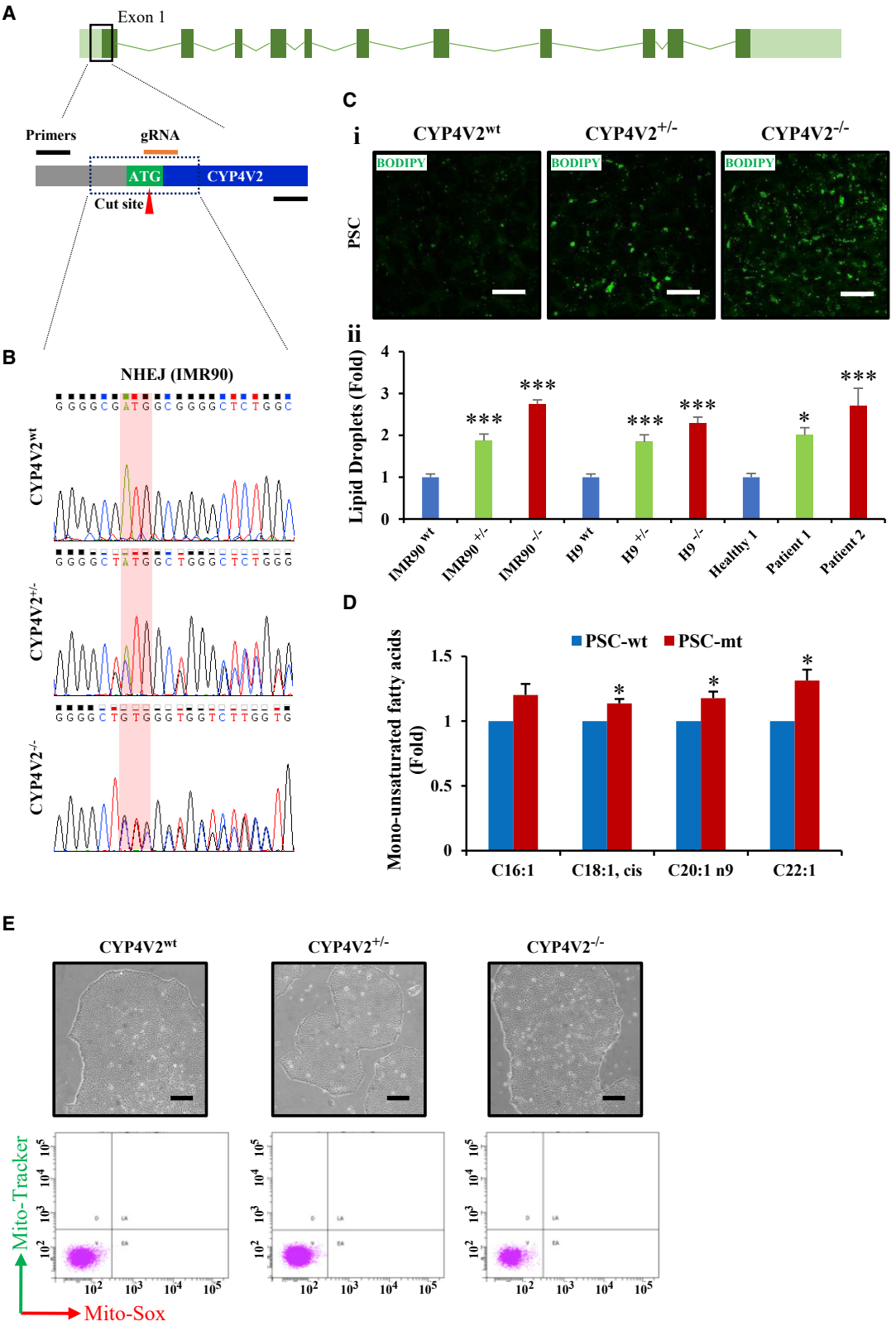

(legend on next page)

were designed to knock out *CYP4V2* in human PSCs, including IMR90 and H9 cells, using CRISPR-Cas9 (Figures 2A and S2A; Table S1).[27] A total of 24 colonies for both IMR90 and H9 cells were picked for genotyping after the neomycin selection. One heterozygote and one homozygote from each IMR90 and H9 colony were selected as the parallel controls to the patient-specific iPSCs (Figures 2B and S2B). The quantitative polymerase chain reaction (qPCR) and immunostaining results indicated the successful gene knockout of *CYP4V2* in both IMR90 and H9 cells (Figures S2C and S2D). Sanger sequencing was used and confirmed that no off-target was found (Figure S2E; Table S1). In this study, a total of nine human PSC lines were established to model BCD, including two of *CYP4V2* wild-type ($CYP4V2^{wt}$) PSCs, two of $CYP4V2^{+/-}$ PSCs, two of $CYP4V2^{-/-}$ PSCs, and three of donor iPSCs (one healthy 1-iPSC and two patients' iPSCs) (Figure S2C). The PSCs with *CYP4V2* knockout and patients' iPSCs were grouped as the CYP4V2 mutant ($CYP4V2^{mt}$) PSCs. The $CYP4V2^{mt}$ PSCs presented lower mRNA levels of *CYP4V2* than did the WTs except for patient 1-PSC in whom *CYP4V2* expression increased, possibly due to a compensatory mechanism or individual difference.[28,29] Nonetheless, the results of fundus images, OCT images, and immunostaining (Figures 1A, 1B, and S2D) indicated the functional defect of the mutant CYP4V2 protein in patients. In this study, we focused on lipid metabolism since BCD was being considered a disease caused by a lipid metabolic disorder.[6,8] Lipid droplets (LDs) were examined by BODIPY-493/503 staining and revealed significantly increased LD accumulations in all $CYP4V2^{mt}$ PSCs compared with the counterpart of $CYP4V2^{wt}$ PSCs (Figure 2C).[30] To gain more information about the fatty acid components, we quantified cellular fatty acids for each of the PSC lines by using gas chromatography-mass spectrometry (GC-MS), which were presented as a form of the mol % ratios.[9,31] Quantities of mono-unsaturated fatty acids (MUFAs), including C18:1 *cis*, C20:1n9, and C22:1, were consistently increased in $CYP4V2^{mt}$ lines, compared to counterparts of the WT PSC lines (Figure S2F). Unexpectedly, omega-3/6 PUFAs were undetectable because of their extremely low concentrations in human PSCs. To provide further comprehensive information about *CYP4V2* mutations and fatty acid homeostasis in PSCs and to minimize interference of genetic background and individual differences, we pooled all the PSCs into $CYP4V2^{wt}$ PSCs and $CYP4V2^{mt}$ PSCs for statistical analysis. Compared to $CYP4V2^{wt}$ PSCs, significantly increased MUFAs were detected in $CYP4V2^{mt}$ PSCs, including oleic acid (C18:1), gondoic acid (C20:1n9), and erucic acid (C22:1) (Figure 2D). Overloaded fatty acids in non-adipose cells, similar to mitochondrial reactive oxygen species (mtROS), have been reported to trigger oxidative stress or lipotoxicity.[32–34] Nonetheless, there was no increase and little difference in the mtROS between $CYP4V2^{wt}$ and $CYP4V2^{mt}$ PSCs measured by fluorescence-activated cell sorting (FACS) (Figure 2E), indicating that PSCs were not sensitive to these distinctly altered fatty acid profiles. Regarding the lipotoxicity, the effect on cell survival, cell growth, and differentiation potential of three germ layers in $CYP4V2^{mt}$ PSCs with the accumulated lipids was unremarkable (Figures 2E, S2G, and S2H).

Fatty Acid Accumulations in $CYP4V2^{mt}$ RPE Cells

To establish a retinal disease model of BCD, functional RPE cells were generated from the above-mentioned three donor iPSCs (healthy 1, patient 1, and patient 2) and six parallel PSC controls using a published protocol for RPE differentiation (Figure S3A).[35] The generated RPE cells exhibited a polygonal, cobblestone-like, and highly pigmented appearance, as measured by positive immunostaining of ZO-1, bestrophin, CRALBP, and RPE65; RPE genes (*MITF* and *TYR*) were increased more than 1,000-fold compared with undifferentiated PSCs. Typical RPE ultrastructure was observed by transmission electron microscopy (TEM), functional phagocytosis of RPE was recorded by the uptake of rhodopsin, and increased transepithelial electrical resistance (TER) levels were evidenced (Figures S3B–S3F). These RPEs were fully functional, mature, and used for further investigation of BCD-RPE phenotypes.

Similarly, $CYP4V2^{mt}$ RPE cells presented significantly decreased levels of *CYP4V2* compared with their WT counterparts except for patient 1-RPE, in whom *CYP4V2* expression increased (Figure S3G). This is consistent with their PSCs (Figure S2C). To visualize the neutral lipids of the cells, six parallel $CYP4V2^{mt}$ and three donor RPE cells were stained with BODIPY-493/503. The results showed significantly accumulated LDs in $CYP4V2^{mt}$ RPE cells but not in $CYP4V2^{wt}$ RPE cells (Figure 3A). Additionally, TEM results revealed that swollen LDs clustered in the cytoplasm of $CYP4V2^{mt}$ RPE cells (Figure S3H). To examine the fatty acid profile, we quantified the total cellular fatty acids by using GC-MS analysis, which were presented as a form of the mol % ratios of different fatty acids.[9,31] We found that quantities of MUFAs and PUFAs, including C16:1, C18:1 *cis*, C18:2 *cis*, C18:3n6, C20:4n6, and C20:5, were consistently increased in all individual $CYP4V2^{mt}$ RPE cells compared with their corresponding $CYP4V2^{wt}$ controls (Figures S3I and S3J). Because RPE degeneration was evident in all BCD patients with various *CYP4V2* mutations, all

Figure 2. Effects of *CYP4V2* Mutation on Human PSCs

(A) Sketch of *CYP4V2* knockout. gRNAs were designed to target the translation start site (ATG) of *CYP4V2*. Primers were designed to cover the cutting sites of gRNA for Sanger sequencing. (B) Genotypes of *CYP4V2* knockout IMR90 cells. The non-homologous end joining (NHEJ) repair was introduced to destroy the targeted ATG. The heterozygote showed ATG and messy peaks, and no ATG was found in the homozygote. (C) Lipid accumulation in all nine PSCs. (i) The representative images show that distinct lipid droplets (LDs) accumulated in $CYP4V2^{mt}$ PSCs stained with BODIPY-493/503 (bright green dots). Scale bars, 25 μm. (ii) Compared with WT PSCs, Lipid is significantly accumulated in $CYP4V2^{+/-}$ and $CYP4V2^{-/-}$ PSCs. A one-way ANOVA and Newman-Keuls test were used: $^{*}p < 0.05$, $^{***}p < 0.0001$; all versus WT (mean ± SEM values, n = 4,000 cells). (D) Increased unsaturated fatty acids in $CYP4V2^{mt}$ PSCs compared to $CYP4V2^{wt}$ PSCs (10 million cells were used in each cell line for GC-MS, and PUFA is undetectable in all nine PSCs). For the data analysis, the mol % was used for individual fatty acids, normalized with the WT control for statistical analysis. A t test (two-tailed) and paired test were used; $^{*}p < 0.05$; all versus PSC-WT (mean ± SEM values, n = 6). (E) No remarkable differences in the morphology and ROS levels between the $CYP4V2^{mt}$ and $CYP4V2^{mt}$ PSCs. Scale bars, 100 μm.

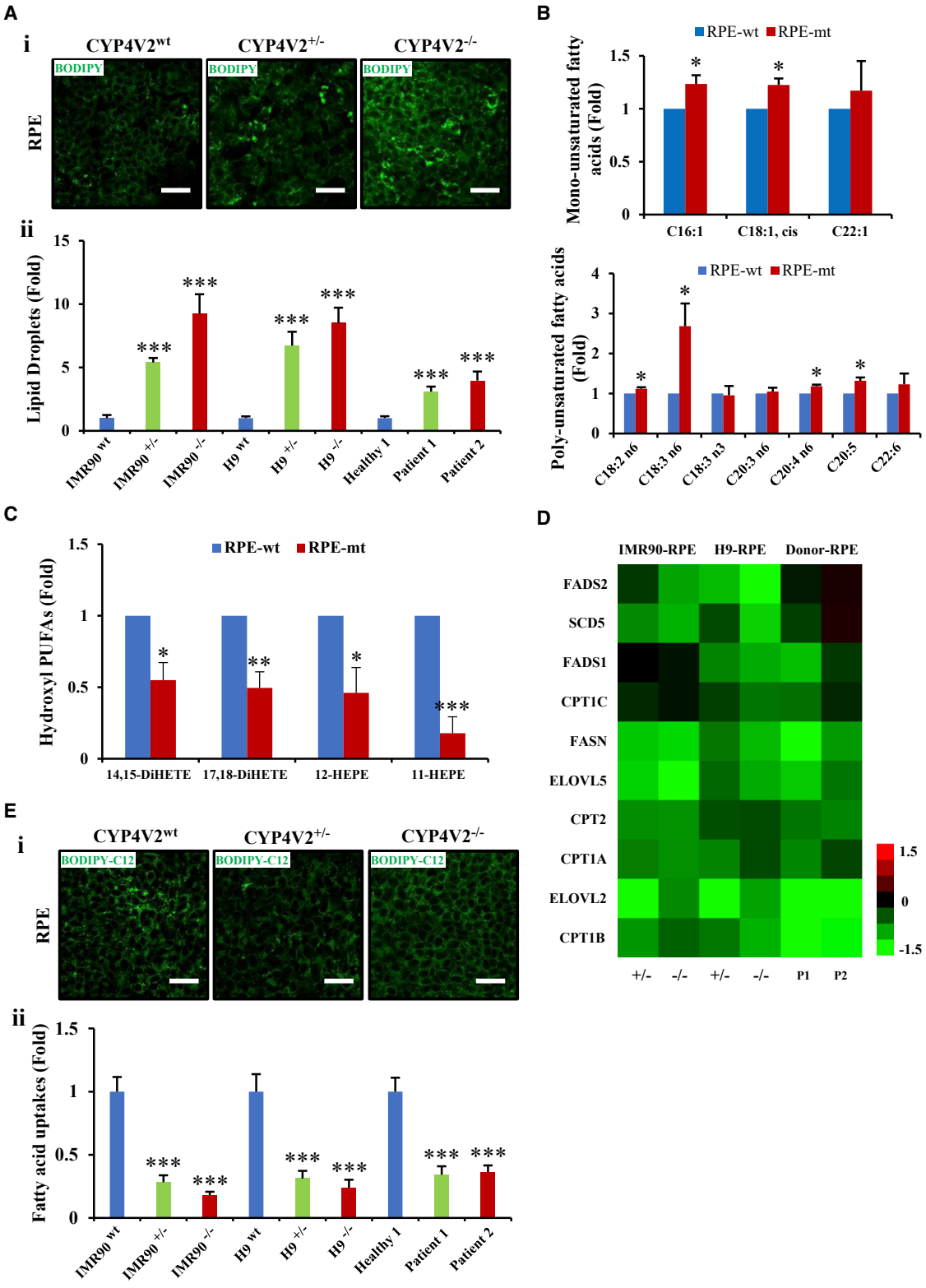

(legend on next page)

CYP4V2^{mt} RPE cells were further pooled together as CYP4V2^{mt} RPE cells in comparison with the WT counterparts to minimize the interference of individual differences and genetic backgrounds.[36,37] Compared to the CYP4V2^{mt}, significantly increased MUFAs were observed in CYP4V2^{mt} RPE cells. More obviously, remarkably accumulated PUFAs were recorded in CYP4V2^{mt} RPE cells, particularly for AA (C20:4n6) and EPA (C20:5) (Figure 3B). CYP4V2 was reported to be associated with fatty acid hydroxylation in fatty acid metabolism.[7] To determine whether the fatty acid accumulations in CYP4V2^{mt} RPE cells were caused by fatty acid synthesis, fatty acid catabolism, or fatty acid uptake, the fatty acid hydroxylation was tested in all CYP4V2^{mt} PRE cells using liquid chromatography-mass spectrometry (LC-MS) first.[38] Only concentrations of hydroxyl PUFAs were significantly decreased in the CYP4V2^{mt} RPE cells compared with the counterparts of CYP4V2^{wt} RPE cells, indicating inhibited fatty acid hydroxylation in both patients' RPE cells and parallel CYP4V2^{mt} RPE cells (Figures 3C and S3K). Next, qPCR results showed that a panel of key genes involved in fatty acid synthesis and catabolism were downregulated in CYP4V2^{mt} RPE cells (Figure 3D).[39,40] Among them, downregulated gene expression of carnitine palmitoyltransferases (CPTs) may suggest impaired fatty acid catabolism in the cells. At last, BODIPY-C12 staining was performed to evaluate the fatty acid absorption of RPE cells.[41] In comparison with CYP4V2^{wt} RPE cells, the mutant presented lower levels of fatty acid uptake (Figure 3E). Our results suggested a fatty acid metabolism disorder in CYP4V2^{mt} RPE cells caused by impaired fatty acid hydroxylation.

Transcriptome Analysis of CYP4V2^{mt} RPE Cells

To gain molecular insights into the *CYP4V2* mutation-induced RPE degeneration, we examined altered gene expression profiles using genome-wide RNA sequencing. Hundreds of differentially expressed genes with at least 1.5-fold changes (FCs) were identified between CYP4V2^{wt} and CYP4V2^{mt} RPE cells (Figures 4A and S4A). Among them, 220 genes were significantly changed in both CYP4V2$^{+/-}$ and CYP4V2$^{-/-}$ IMR90-RPE cells, 253 genes in both the CYP4V2$^{+/-}$ and CYP4V2$^{-/-}$ H9-RPE group, and 352 genes in patients' RPE groups. Next, gene set enrichment analysis (GSEA) analysis indicated that major enriched signal pathways of CYP4V2$^{-/-}$ RPE cells were prominently involved in fatty acid metabolism (i.e., upregulated lipid storage and downregulated lipid biosynthesis), as well as oxidative stress (i.e., a positive response to ROS and downregulated ROS biosynthesis) and apoptosis (i.e., upregulated p53-independent apoptosis) (Figures 4B, S4B, and S4D).[42] Remarkably, p53-dependent pathways were downregulated, but p53-independent apoptosis and the typical gene expression involved in oxidative stress were over-represented in CYP4V2$^{-/-}$ H9 and IMR90-derived RPE cells.[43] It is remarkable that the differential genes of CYP4V2$^{-/-}$ RPE cells were predominantly mapped to fatty acid metabolism, oxidative stress, and apoptosis in volcano plots (Figures 4C, 4D, and S4C). These observations are evident too in all CYP4V2^{mt} RPE cells (Table S2). However, the similar result was not found in CYP4V2$^{-/-}$ PSCs. These findings suggested that the absence of the *CYP4V2* disturbed fatty acid metabolism and induced oxidative stress and apoptosis are only specifically sensitive to human RPE cells, but not PSCs.

Mitochondrial Stress and Apoptosis of CYP4V2^{mt} RPE Cells

The overload of fatty acid can trigger the oxidative stress to damage cells,[32,44,45] which was also supported by our transcriptome data (Figure 4). To understand whether excessive fatty acid induced mtROS in RPE cells, we determined the mtROS level in RPE cells by co-staining with MitoTracker and MitoSOX, sensitive markers to define mitochondrial oxidative status first.[45,46] Compared with the CYP4V2^{wt} counterparts, there was a significant increase of mtROS in CYP4V2^{mt} RPE cells (Figure 5A). Next, the mitochondrial respiratory function was examined by measuring the mitochondrial oxygen consumption rate (OCR) in live RPE cell cultures.[47] The significantly lower OCR was recorded in the CYP4V2^{mt} RPE cells in comparison to the counterpart of CYP4V2^{wt} RPE cells, which presented a lowest level observed in homogeneous CYP4V2^{mt} RPE cells (Figure 5B). This suggested a damaged mitochondrial function in CYP4V2^{mt} RPE cells with fatty acid overload.[47] It was reported that cells died from the fatty acid overload-caused oxidative stress.[44] The increased dead cells were observed in the culture medium of all CYP4V2^{mt} RPE cells (Figure S5A). To confirm the cell apoptosis, the cultured RPE cells were harvested for an annexin V/propidium iodide (PI) assay. Significantly increased annexin V-positive cells and a few PI-positive cells were found, indicating early cell apoptosis in CYP4V2^{mt} RPE cells (Figure 5C).[48,49] In addition to the mitochondrial oxidative stress, the signaling pathway involved in endoplasmic reticulum (ER) stress was linked to lipotoxicity-induced apoptosis of non-adipose cells.[50]

Figure 3. Fatty Acid Accumulations in CYP4V2 Mutant RPE Cells

(A) Lipid accumulation in all nine RPE cells. (i) The representative images show that distinct LDs accumulated in CYP4V2^{mt} RPE stained with BODIPY-493/503 (bright green dots). Scale bars, 25 μm. (ii) Compared with WT RPE cells, lipid is significantly accumulated in CYP4V2$^{+/-}$ and CYP4V2$^{-/-}$ PRE cells. A one-way ANOVA and Newman-Keuls test were used: *p < 0.05, ***p < 0.0001; all versus WT (mean ± SEM values, n = 4,000 cells). (B) Compared to the CYP4V2^{wt} RPE cells, increased unsaturated fatty acids and PUFAs were found in the CYP4V2^{mt} RPE cells. 10 million cells were used in each cell line for GC-MS. For data analysis, the mol % was used for individual fatty acid, normalized with the WT control. A t test (two-tailed) and paired test were used: *p < 0.05; all versus WT (mean ± SEM values, n = 6). (C) Decreased hydroxyl PUFAs in CYP4V2^{mt} RPE cells. 10 million cells were used in each cell line. The mol % was used for individual fatty acid, normalized with the WT control. A t test (two-tailed) and paired test were used: *p < 0.05, **p < 0.01, ***p < 0.001; all versus RPE-WT (mean ± SEM values, n = 6). (D) Gene expression level of key markers involved in fatty acid metabolism. qPCR results indicated genes involved in fatty acid synthesis and catabolism were generally downregulated in CYP4V2^{mt} RPE cells. +/−, CYP4V2$^{+/-}$versus CYP4V2^{wt}; −/−, CYP4V2$^{-/-}$ versus CYP4V2^{wt}; P1, patient 1 versus healthy 1; P2, patient 2 versus healthy 1. (E) Fatty acid uptake in all nine RPE cells. (i) The representative images show reduced fatty acid uptake in CYP4V2^{mt} RPE cells stained with BODIPY-C12 (bright green dots). Scale bars, 25 μm. (ii) Compared with WT RPE cells, fatty acid uptake is significantly increased in CYP4V2$^{+/-}$ and CYP4V2$^{-/-}$ PRE cells. A one-way ANOVA and Newman-Keuls test were used: ***p < 0.0001; all versus WT (mean ± SEM values, n = 4,000 cells).

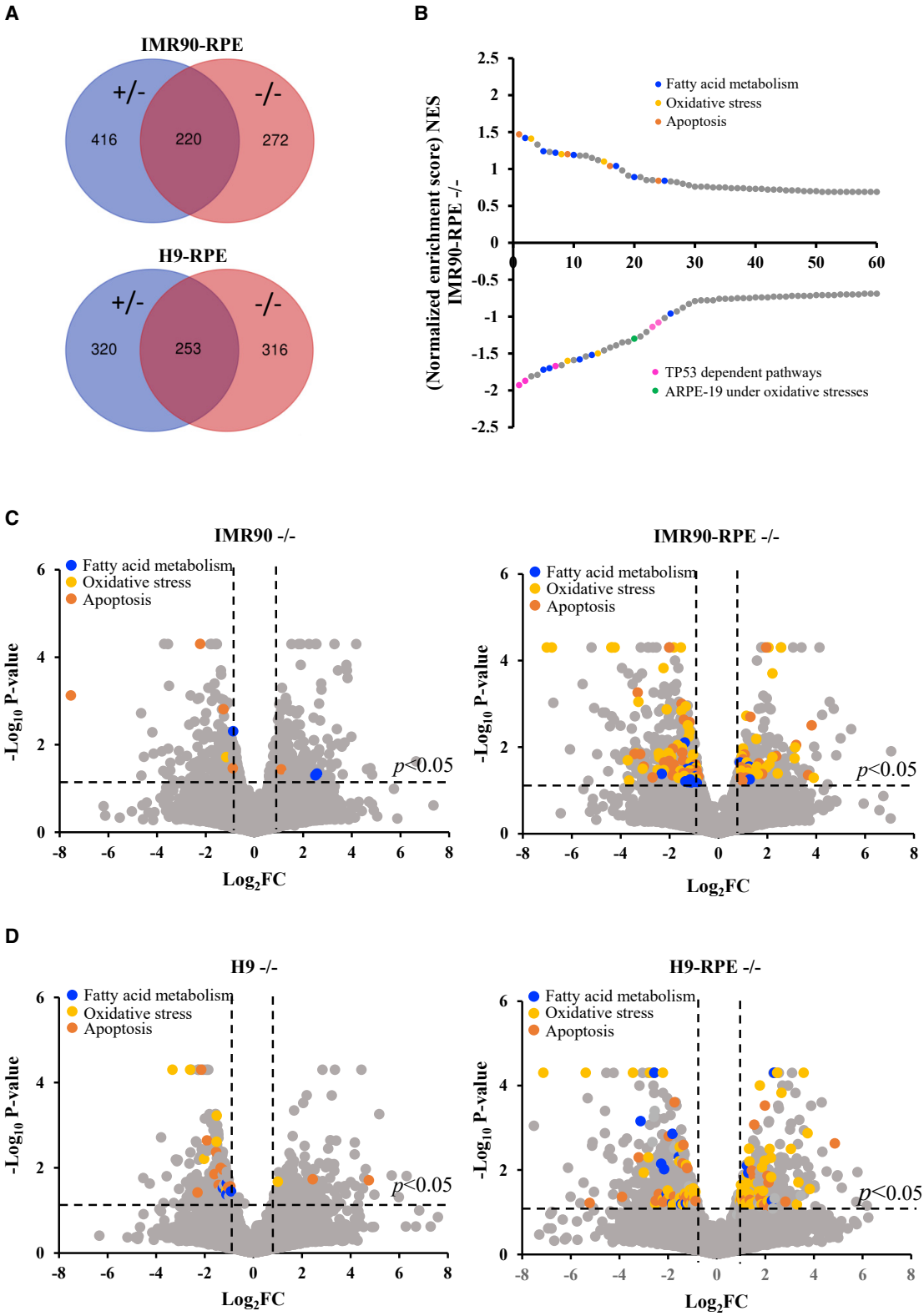

(legend on next page)

We therefore examined the mRNA expression of a panel of key genes involved in these pathways using qPCR. Compared with their WT counterparts, no obviously upregulated gene involved in the ER-stress pathway was found in the CYP4V2^{mt} RPE cells (Figure S5B; Table S3). Apoptosis genes, including *BBC3*, were upregulated in CYP4V2^{mt} RPE cells, but *BCL2*, *BCL2L1*, *BIRC2*, and *TP53* genes were significantly downregulated (Figure 5D; Table S3), indicating that a p53-independent apoptosis was predominantly activated in response to fatty acid accumulation-provoked mitochondrial stresses.[51,52] Additionally, the remarkable release of cytochrome *c* from mitochondria was found in the CYP4V2^{mt} RPE cells but not in the CYP4V2^{wt} RPE cells (Figure 5E).[53] At last, the results of western blotting indicated the activated caspase-9 cascade in CYP4V2^{mt} RPE cells, as well as further evidence of increased mitochondrial damage and apoptosis in CYP4V2^{mt} RPE cells (Figure 5F).[54]

PUFA Administration Sensitively Induces Cell Death in CYP4V2^{mt} RPE Cells

Saturated and unsaturated fatty acids assume different roles in humans and in retinal function. It is therefore important to determine which compositions of fatty acids are sensitive and toxic to RPE degeneration.[46,55] No oxidative stress and cell death were found in CYP4V2^{mt} PSCs with no PUFA detection (Figure 2), but increased oxidative stress and cell apoptosis were accompanied by accumulated PUFA in CYP4V2^{mt} RPE cells (Figures 3 and 5). This implies that the PUFA overload might be a potential trigger of lipotoxicity-caused RPE degeneration in BCD patients.[56] Dose-escalation experiments revealed distinct sensitivities of three CYP4V2^{wt} RPE cells to 1 week of challenge by different fatty acids, including the saturated fatty acids (SFAs).[57] In the SFA-treated group, viability of RPE cells was not affected by treatment with myristic acid (MA, C14:0), palmitic acid (PA, C16:0), or stearic acid (SA, C18:0) until a high concentration of 200 μM was used (Figure S6A). In contrast, in the PUFA-treated group,[58] administration of PUFAs separately, including linoleic acid (LA, C18:2), α-linolenic acid (ALA, C18:3), AA, and EPA, could induce cell death in all human RPE cells, even at an extremely low concentration (20 μM) (Figures 6A and 6B). Additionally, LDs were increased in CYP4V2^{wt} RPE cells following treatments with AA and EPA (Figure 6C). To verify whether PUFAs coupled with enhanced mitochondrial oxidative stress are toxic to RPE cells, RPE cells were treated with AA and EPA to detect mtROS as well. Both AA- and EPA-treated groups displayed significantly higher levels of mtROS compared with untreated controls, with the highest levels evident in EPA-treated groups (Figure 6D). This suggested that PUFA-triggered oxidative stresses could cause the death of normal RPE cells. In addition, all CYP4V2^{wt} and CYP4V2^{mt} RPE cells were challenged with continuous exposures to AA and EPA (40 μM and 7 days). Dramatically enhanced cell death was evident in the CYP4V2^{mt} RPE cells compared with the CYP4V2^{wt} counterparts (Figure 6E).

Functional Restoration of CYP4V2^{mt} RPE Cells in AAV2-CYP4V2 Gene Therapy

To explore the feasibility of gene therapy for BCD, a vector of AAV2-carrying functional *CYP4V2* (AAV2-CYP4V2) was constructed and characterized by Sanger sequencing (Figure S7A). One week after AAV infections, the mRNA and protein levels of *CYP4V2* were measured and found to be significantly increased in CYP4V2$^{-/-}$ RPE cells (Figure S7B). The functions of three CYP4V2$^{-/-}$ RPE cells were examined following the AAV2-CYP4V2-mediated gene therapy. First, a significant decrease in fatty acid accumulation was detected in CYP4V2$^{-/-}$ RPE cells upon the gene therapy (Figure 7A). Second, the damaged mitochondria of CYP4V2$^{-/-}$ RPE cells were largely recovered, signified by reduced mtROS and improved mitochondrial respiration (Figures 7B and 7C). Importantly, cell death of RPE was dramatically reduced in CYP4V2^{mt} RPE cells after treatment with AAV2-CYP4V2 (Figures S7C and 7D). The AAV2-CYP4V2-treated CYP4V2$^{-/-}$ RPE cells were also again challenged by continuous exposure to AA and EPA. As expected, death of these RPE cells was remarkably reduced as well (Figure 7E). Of note, AAV2-CYP4V2 therapy could largely recover the suppressed hydroxyl fatty acids and reduce the enhanced PUFA in CYP4V2$^{-/-}$RPE cells (Figures 7F and 7G), indicating that AAV2-CYP4V2 gene therapy could preserve RPE viability and recover RPE function from *CYP4V2* mutations.

DISCUSSION

The lack of appropriate disease models and patients' RPE cells has made it difficult to determine how *CYP4V2* mutations induce RPE degeneration of BCD patients. Increased crystalline depositions have been observed in a mouse model. Unfortunately, the mouse model with absence of *Cyp4v3*, the murine ortholog to *CYP4V2*, mainly exhibits impaired photoreceptors, not RPE degeneration, unlike in humans with BCD, where the RPE is the primary lesion site.[10] Recently, Hata et al.[14] used iPSC-derived RPE cells from BCD patients and reported increased cholesterol, impaired autophagy flux, and lysosomal dysfunction in RPE. They reported that some proteins related to autophagy were upregulated in patient-RPE cells; however, activation of the autophagy pathway is not attenuated upon cholesterol reduction treatment, implying the possibility that other mechanisms are involved in RPE degeneration in BCD patients. In addition, because of the lack of isogenic controls, the possible bias from

Figure 4. Transcriptome Data Analysis

(A) Differential genes (fold changes greater than 1.5) in respective iPSC- and H9-derived RPE. +/−, CYP4V2$^{+/-}$ versus CYP4V2^{wt}; −/−, CYP4V2$^{-/-}$ versus CYP4V2^{wt}. (B) GSEA analysis of the functional relevance of differential genes in CYP4V2$^{-/-}$ IMR90 RPE cells. Pathways involved in fatty acid metabolism, oxidative stress, and apoptosis were enriched. −/−, CYP4V2$^{-/-}$ versus CYP4V2^{wt}. (C) Volcano plots of DEGs in parallel IMR90 cells and their derived RPE cells. DEGs mapped to fatty acid metabolism, oxidative stress, and apoptosis were predominantly enriched in CYP4V2$^{-/-}$ IMR90-RPE cells, but not in CYP4V2$^{-/-}$ IMR90 cells. −/−, CYP4V2$^{-/-}$ versus CYP4V2^{wt}. (D) Volcano plots of DEGs in parallel H9 and their derived RPE controls. DEGs mapped to fatty acid metabolism, oxidative stress, and apoptosis were predominantly found in CYP4V2$^{-/-}$ H9-RPE cells, but not in CYP4V2$^{-/-}$ H9 cells. −/−, CYP4V2$^{-/-}$ versus CYP4V2^{wt}.

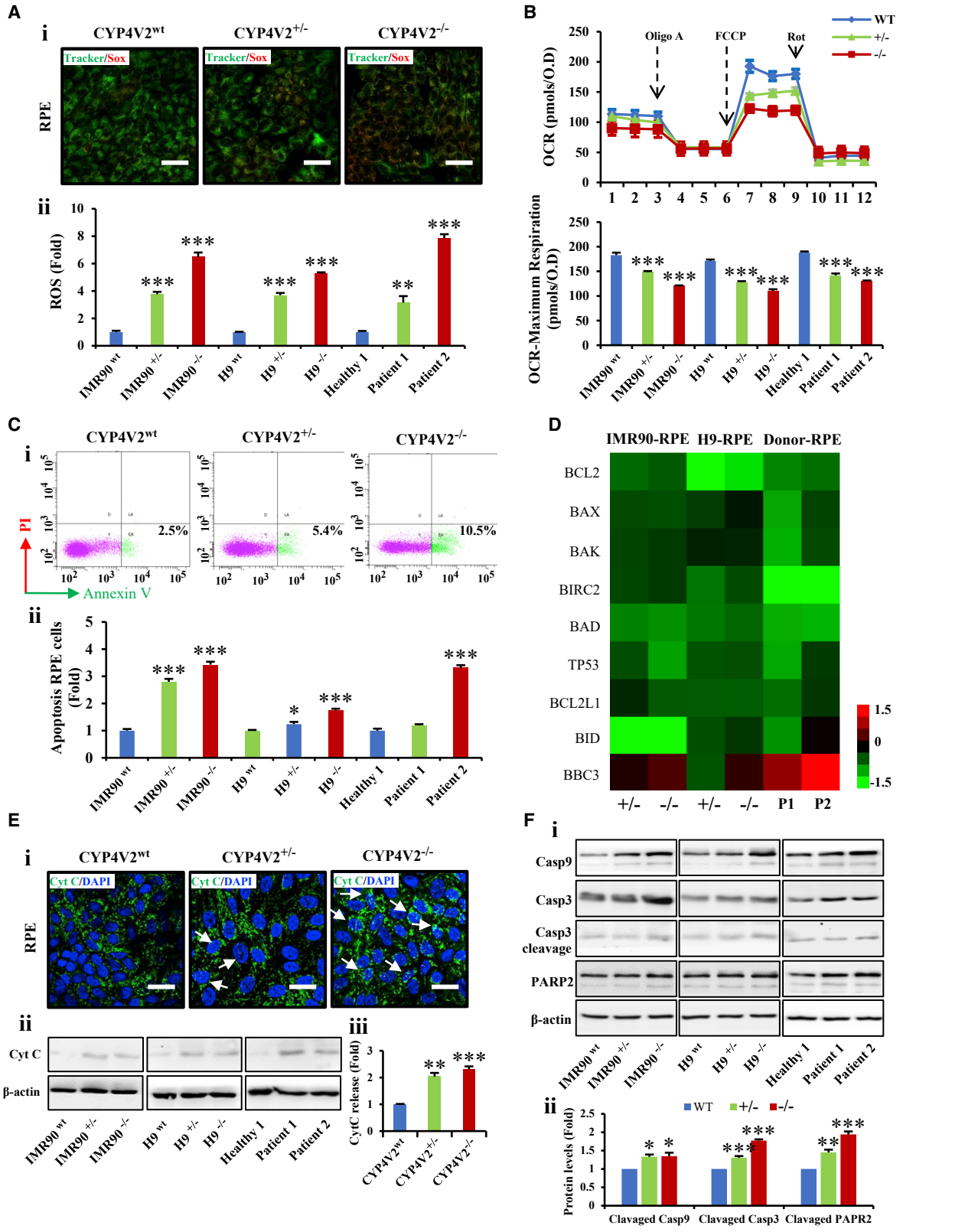

(legend on next page)

individual differences may also have influenced the results.[59] Importantly, there is no clinical report indicating a high cholesterol level in a BCD patient's serum. In contrast, increased fatty acids were reported in the serum of BCD patients.[9] Indeed, human retina contains rich components of fatty acids, and homeostasis of fatty acids is essential for retinal functions, including oxidation.[55] BCD is an autosomal recessive disorder. It was reported that pathological mutations of *CYP4V2* were not found in coding regions or were difficult to be identified in the second allele in some patients with BCD.[19–23] The *CYP4V2* mutations might be presented in other forms, i.e., CNVs, mutations in non-coding regions, or structural mutations. In our study, similar situations also happened in patient 1 who displayed only one point mutation in the coding region of *CYP4V2* in the first allele, but not found so in the second allele. To minimize the possible interference from individual variants and unknown mutations in patients' iPSCs,[11] we used commercial PSCs with genome editing, patient-specific iPSCs, and their derived RPE cells for cellular fatty acid profiling and transcriptome analysis, and identified a mechanism wherein *CYP4V2* mutation-induced RPE degeneration in BCD is attributed to mitochondrial damage triggered by excessive PUFA accumulation.

In humans, PUFA is low in concentration, but is essential for the roles in molecular signal transduction and hormone synthesis, and relies more on the metabolic ways, including the peroxisome and cytochrome P450 superfamilies.[60–63] It has been demonstrated that *CYP4V2* is functional in the hydroxylation of some fatty acids for omega oxidation, but there is no direct evidence to support its role in the fatty acid metabolism in human retina.[7,8] All previous studies, including increased PUFAs in BCD patients' serum, strongly suggested the correlation among *CYP4V2* mutations, the fatty acid metabolic disorder, and RPE degeneration in patients with BCD.[4,5,7–9,15] In our study, we determined that human CYP4V2^{mt} PSCs contained increased MUFAs (Figure 2D), and CYP4V2^{mt} RPE cells contained increased PUFAs (Figure 3B), which provided definitive evidence of a fatty acid metabolic disorder in BCD patients' RPE. These results agree with previous reports of notably increased PUFAs in CYP4V2^{mt} HepG2 cells, serum of BCD patients, and in an animal model.[8–10] Indeed, *CYP4V2* is expressed at a low level in normal PSCs but at a higher level in RPE cells, implying its critical functions for RPE cells.[14] The PUFA concentration was too low to be undetected in CYP4V2^{mt} and CYP4V2^{wt} PSCs, but high levels of PUFAs and low levels of hydroxyl-PUFAs were detected in CYP4V2^{mt} RPE cells, indicating that excessive PUFAs are specifically accumulated only in CYP4V2^{mt} RPE cells (Figures 3B and 3C). Additionally, our studies demonstrated that increased PUFAs with decreased hydroxyl-PUFAs can be rescued by introducing functional *CYP4V2* into CYP4V2^{mt} RPE cells (Figures 7F and 7G), indicating its functions in PUFA hydroxylation, and PUFA accumulation induced by *CYP4V2* mutation triggered dysfunction of PUFA hydroxylation in human RPE cells. This is also further supported by the consistent results of increased PUFA, decreased PUFA hydroxylation, and decreased fatty acid uptake and synthesis recorded in CYP4V2^{mt} RPE cells (Figure 3).

Dietary PUFAs are widely accepted against metabolic diseases, including cardiovascular disorders, tumors, and diabetes. However, certain cell types, including retinal cells, are toxicity-sensitive to excessive PUFAs, i.e., EPA and AA.[46,64] Recently, clinical research has questioned the benefits of PUFA in the human retina. Christen et al.[65] revealed that over-uptake of omega-3 fatty acid increased the risk of macular degeneration in elderly humans. Tanito et al.[66] proposed the dual role of PUFA in retinal degeneration. However, there is no study to provide direct information about the negative part of PUFA in human retinal cells. Hence, there is no report to clarify the mechanisms of PUFA overload-induced lipotoxicity in human RPE cells.[66,67] In our study, no PUFA, mitochondrial stress, and lipotoxicity was detected in CYP4V2^{mt} PSCs (Figure 2). In contrast, when PSCs were induced into RPE cells, the polarized CYP4V2^{mt} RPEs presented enhanced PUFAs (LA, ALA, AA, and EPA) accompanied by increased cell death (Figures 3 and 5), highlighting that RPE cells, but not human PSCs, are particularly sensitive to the *CYP4V2* mutation-provoked PUFA accumulations. Our transcriptomic analysis indicated the close association of fatty acid metabolism, oxidative stresses, and apoptosis in CYP4V2^{mt} RPE cells (Figure 4). Given that the RPE is a highly

Figure 5. Mitochondrial Damage-Triggered Apoptosis in CYP4V2^{mt} RPE Cells

(A) Enhanced mitochondrial ROS (mtROS) in CYP4V2^{mt} RPE cells. (i) Representative images show increased mtROS in CYP4V2^{mt} RPE cells stained with MitoTracker and MitoSOX. Scale bars, 25 μm. (ii) Compared with the WT RPE cells, mtROS is significantly increased in CYP4V2$^{+/-}$ and CYP4V2$^{-/-}$ PRE cells. A one-way ANOVA and Newman-Keuls test were used: **p < 0.001, ***p < 0.0001; all versus WT (mean ± SEM values, n = 4,000 cells). (B) Decreased functions of mitochondrial respiration in CYP4V2^{mt} RPE cells. The OCR was normalized based on the protein concentration of the cells. wt, CYP4V2^{wt}; +/−, CYP4V2$^{+/-}$; −/−, CYP4V2$^{-/-}$. A one-way ANOVA and Newman-Keuls test were used: ***p < 0.0001; all versus WT (mean ± SEM values, n = 3). (C) Annexin V staining and flow cytometry analysis. (i) Representative images show increased annexin V-positive population in CYP4V2^{mt} RPE cells. (ii) Compared with WT RPE, the annexin V-positive population is significantly increased in CYP4V2$^{+/-}$ and CYP4V2$^{-/-}$ PRE cells. A t test (two-tailed) and paired test were used: *p < 0.05, ***p < 0.001; all versus WT (mean ± SEM values, n = 3). (D) Gene expression level of key markers involved in apoptosis. qPCR results indicated genes involved in the p53 signaling pathway were generally downregulated in CYP4V2^{mt} RPE cells, but the gene involved in cytochrome *c* release was upregulated. +/−, CYP4V2$^{+/-}$versus CYP4V2^{wt}; −/−, CYP4V2$^{-/-}$ versus CYP4V2^{wt}; P1, patient 1 versus healthy 1; P2, patient 2 versus healthy 1. (E) Release of cytochrome *c*. (i) Representative images show increased release of cytochrome *c* in CYP4V2^{mt} RPE cells (arrows indicated cytochrome *c* relocated in the cell nucleus). Scale bars, 15 μm. (ii) Western blot results showed increased cellular cytochrome *c* released in CYP4V2^{mt} RPE cells. 40 μg per lane, 1.5-mm comb with 10 spacers. (iii) Statistical analysis of the western blot. A significantly increased cytochrome *c* release in CYP4V2^{mt} RPE cells is shown. A t test (two-tailed) and paired test were used: **p < 0.01, ***p < 0.001; all versus WT (mean ± SEM values, n = 3). (F) Western blotting of caspase cascade. (i) Representative images show increased expressions of caspase-relevant proteins in CYP4V2^{mt} RPE cells. 40 μg per lane, 1.5 mm comb with 10 spacers. (ii) Significantly increased cleavage casp9, casp3, and PAPR2 in CYP4V2^{mt} RPE cells was quantified from western blotting results. A t test (two-tailed) and paired test were used: *p < 0.05, **p < 0.01, ***p < 0.001; wt, CYP4V2^{wt}; +/−, CYP4V2$^{+/-}$; −/−, CYP4V2$^{-/-}$, all versus WT (mean ± SEM values, n = 3).

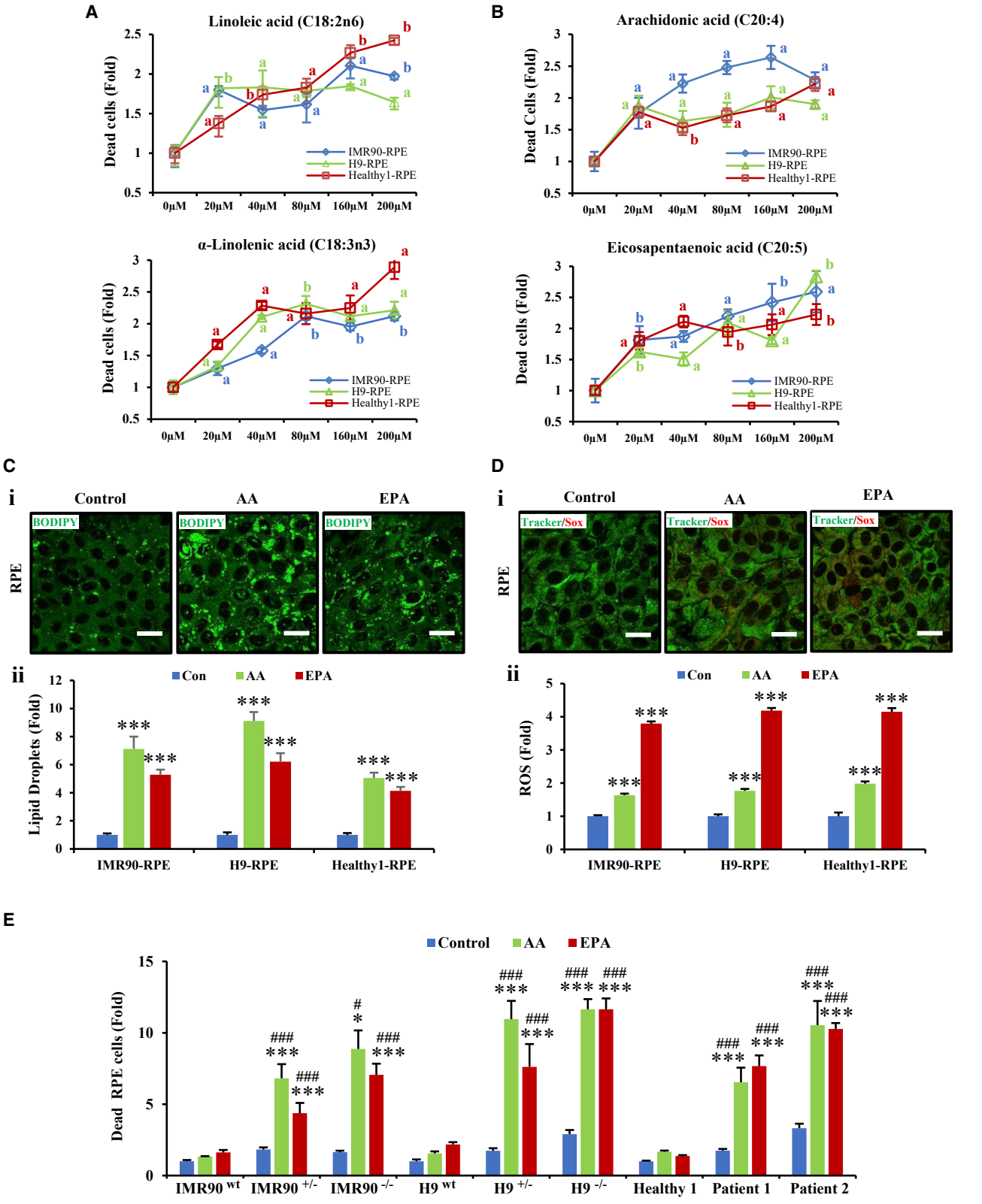

(legend on next page)

metabolically active monolayer of cuboidal cells continuously bombarded by high levels of oxidants, there is compelling evidence that mitochondrial dysfunction is a hallmark of RPE degeneration.[68] Remarkable increases of mtROS and mitochondria damage were found in CYP4V2^{mt} RPE cells accompanied by cell apoptosis, suggesting PUFA overload-induced lipotoxicity (Figures 5A–5C). The upregulated p53 pathway and cytochrome *c* release are strongly associated with oxidative stress in human cells.[69,70] In our studies, downregulated *TP53*, cytochrome *c* release, and activated caspase-9 cascade (Figures 5D–5F) indicated that the PUFA-induced mitochondrial stress provoked a p53-independent apoptosis in CYP4V2^{mt} RPE cells. Our data provide important evidence of the dual roles of PUFA in either maintaining cell homeostasis or inducing cell degeneration, dependent on different conditions and cell types.

To further verify the central role of excessive PUFAs in potentiating degeneration, both SFAs and PUFAs were used to stress normal RPE cells. Accordingly, an increased number of dead cells were only found in all PUFA-treated RPE cells after 1 week of treatment (Figures S5A, 6A, and 6B). Because BCD is a chronic disease, we continually treated healthy RPE cells with PUFAs at a low concentration relative to their physiological level in human plasma.[71] PUFAs are a type of fatty acids that contain more than two unsaturated olefinic bonds, and thus are oxidized or peroxided easily *in vivo*.[72] A persistent overload of PUFAs in the cells is toxic and damages the organelles, including mitochondria, because of the sharp increase in ROS generated by the PUFA oxidation or peroxidation.[46] In our studies, fatty acid accumulations accompanied with significantly increased mtROS were recorded in all PUFA-treated RPE cells (Figures 6C and 6D). The increased apoptosis of PUFA-treated CYP4V2^{mt} RPE cells strongly supported the potency of excessive PUFAs in inducing RPE degeneration in BCD (Figure 6E). These results were consistent with the typical features of lipotoxicity and accompanied by oxidative stresses and cell death, providing significant information for the dietary management of BCD patients in controlling clinical disease.[33,44,50,73] Importantly, AAV2-mediated gene therapy offers potential for the clinical treatment of hereditary retinal diseases.[16] The introduction of AAV2-CYP4V2 gene therapy largely preserved RPE viability, reduced PUFA concentration and accumulation, ameliorated mitochondrial stress, and enabled recovery of RPE functions, offering a great potential of gene therapy for the treatment of BCD in the future (Figure 7).

In summary, using patients' and parallel CYP4V2^{mt} PSCs as disease models, we identified a disrupted fatty acid homeostasis in human RPE cells with *CYP4V2* mutations. *CYP4V2* mutations impaired PUFA hydroxylation, and PUFA accumulation in turn induced mitochondrial damage, indicating a central role in potentiating BCD-RPE degeneration. In addition, correction of *CYP4V2* mutation with functional AAV2-based gene therapy appears to be a feasible strategy to treat BCD.

MATERIALS AND METHODS

Fundus and OCT Examination

Fundus images were taken by a Topcon TRC-50DX mydriatic retinal camera, and spectral-domain OCT images of macula scans were taken by Heidelberg Spectralis OCT.

PBMC Isolations

Donors' blood was collected into tubes containing heparin and gently transferred to 50-mL centrifuge tubes containing Ficoll-Paque after dilution with same volume of PBS. Then, the middle layer of cells was collected for the next experiments after centrifugation (400 × *g*, 40 min).

iPSC reprogramming

The iPSCs were reprogrammed from adult PBMCs.[25,26] Briefly, PBMCs were isolated by Ficoll-Paque (GE Healthcare) and cultured in mononuclear cell (MNC) medium to induce proliferation of MNCs. Then, episomal vectors (Addgene) expressing four Yamanaka factors were transfected into MNCs by a Lonza 4D-Nucleofector. After 2 days of recovery in MNC medium, cells were cultured on a Geltrex-coated tissue culture plate to induce iPSC reprogramming. Essential 8 (Thermo Fisher Scientific) medium was changed every 2 days. The iPSC clones generally emerged after approximately 2 weeks, which could be passaged for further studies.

ALP Staining

The iPSCs were cultured on cover slides and for 3 days, then fixed with 4% paraformaldehyde (PFA). After washing with PBS, the cover slides were covered by the prepared staining reagent from the ALP staining kit. 15 min later, the reagent was removed, and the cells were observed and recorded by using a normal light microscope.

Figure 6. PUFAs Treatment Sensitively Induced Apoptosis in CYP4V2^{mt} RPE Cells

(A) Killing curves of CYP4V2^{wt} RPE cells upon linoleic acid (C18:2n6) and α-linolenic acid (C18:3n3) treatments. Significantly increased cell death in the RPE cells with fatty acid treatments from the concentration of 20 μM. A t test (two-tailed) and paired test were used: $^{a}p < 0.05$, $^{b}p < 0.01$; all versus 0 μM (mean ± SEM values, n = 3). (B) Killing curves of CYP4V2^{wt} RPE cells upon arachidonic acid (AA, C20:4) and eicosapentaenoic acid (EPA, C20:5) treatments. Significantly increased cell death in the RPE cells with fatty acid treatments from the concentration of 20 μM is shown. A t test (two-tailed) and paired test were used: $^{a}p < 0.05$, $^{b}p < 0.01$; all versus 0 μM (mean ± SEM values, n = 3). (C) Fatty acid accumulation of CYP4V2^{wt} RPE cells upon AA and EPA treatments. (i) Representative images show increased LDs in CYP4V2^{wt} RPE cells stained with BODIPY-493/503. Scale bars, 15 μm. (ii) Compared with the untreated groups, LDs were significantly increased in PRE cells upon AA and EPA treatments. A one-way ANOVA and Newman-Keuls test were used: $^{***}p < 0.0001$; BSA groups were set as control (Con), all versus control (mean ± SEM values, n = 4,000). (D) mtROS staining of CYP4V2^{wt} RPE cells upon AA and EPA treatments. (i) Representative images show increased mitROS in CYP4V2^{wt} RPE cells upon AA and EPA treatments, stained with MitoTracker and MitoSOX. Scale bars, 15 μm. (ii) Compared with the untreated group, mtROS were significantly increased in PRE cells treated with AA and EPA. Enhanced mtROS in RPE cells upon AA and EPA treatments. A one-way ANOVA and Newman-Keuls test were used: $^{***}p < 0.0001$; BSA groups were set as control (Con), all versus control (mean ± SEM values, n = 4,000). (E) Sharply increased cell death in CYP4V2^{mt} RPE cells upon AA and EPA treatments. A one-way ANOVA and Newman-Keuls test were used: $^{*}p < 0.01$, $^{***}p < 0.0001$; all versus WT; $^{\#}p < 0.01$, $^{\#\#\#}p < 0.0001$; all versus control (mean ± SEM values, n = 3).

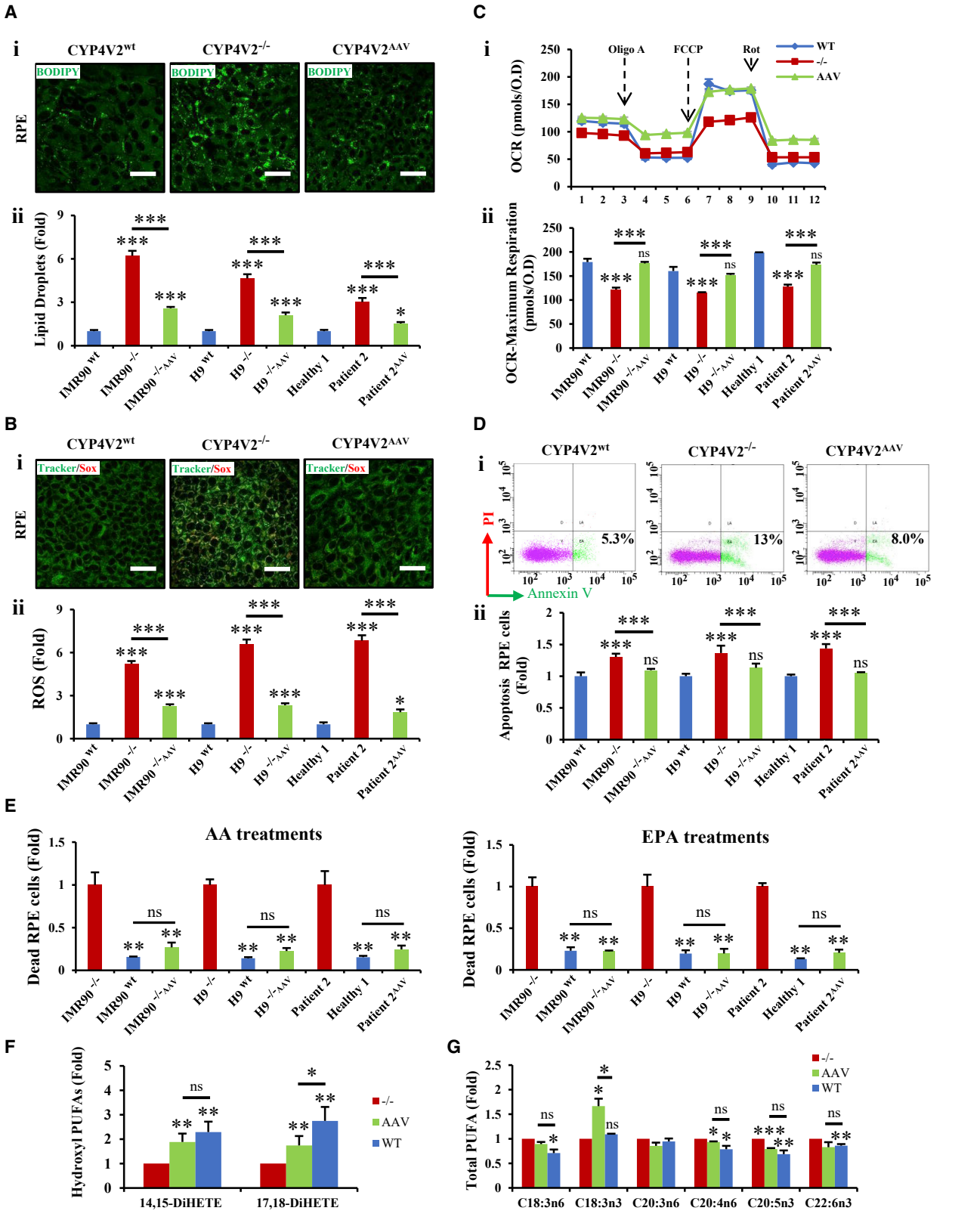

(legend on next page)

Teratoma Formation and H&E Staining

Confluent iPSCs were collected in DMEM/F12 basal medium and were injected subcutaneously into the SCID mice. Normally, the teratoma appears in 3 months, which can be collected and fixed in the formalin for the tissue section. For H&E staining, the paraffin sections were treated with xylene and alcohol for deparaffinization and rehydration. After 8 min of hematoxylin staining, the sections were washed with distilled water again and followed with the eosin staining for 30 s to 1 min. At last, the sections can be mounted for the observations by using a normal light microscope after the dehydration of alcohol.

Knockout CYP4V2 Gene by CRISPR-Cas9

To knock out *CYP4V2* in human PSCs, gRNAs were designed to destroy the transcript start site. After optimization of cutting efficiencies by a Surveyor assay (Integrated DNA Technologies), the gRNA was transfected into 1 million PSCs by a Lonza 4D-Nucleofector (Lonza) together with Cas9 plasmid (Addgene). Cells were cultured on Geltrex-coated 10-cm culture dishes for drug selection of neomycin (Thermo Fisher Scientific) (175 μg/mL for IMR90 cells and 200 μg/mL for H9 cells). The recovered single clones were picked and expanded for genotyping. A total of nine PSCs were used for functional studies, including healthy 1-iPSC, patient 1-iPSC, patient 2-iPSC, H9-iPSC, H9-CYP4V2$^{+/-}$-iPSC, H9-CYP4V2$^{-/-}$-iPSC, IMR90-iPSC, IMR90-CYP4V2$^{+/-}$-iPSC, and IMR90-CYP4V2$^{-/-}$-iPSC.

PCR

For normal PCR, 50 μL of reaction system was prepared using 25 μL of PCR premix Taq, 2 μL of forward/reverse primers (10 μM), 100 ng of template, and 20 μL of deionized water. To amplify the targeted products, the following reaction conditions were used: denaturation at 98°C for 10 s, annealing at 55°C for 10 s (decided by different primers), and extension at 72°C for 1 min/kb, 35 cycles. When the reactions were finished, the PCR products were detected by using agarose gel.

Real-Time PCR

To detect the gene expressions, 2 μL of cDNA was used as a template for real-time PCR. The detailed reaction system was prepared for each reaction: SYBR premix (10 μL), forward primer (0.8 μL, 10 μM/μL), reverse primer (0.8 μL, 10 μM/μL), ROX reference dye (0.4 μL), template (cDNA, 2 μL), and distilled water (2 μL). Then, the PCR was run in the StepOnePlus real-time PCR system with a two-step method: denaturation at 95°C for 5 s, annealing at 60°C for 31 s. To detect CNVs in patients, 11 pairs of primers were used to amplify all exons of *CYP4V2* using *GPR15* and *ZNF80* as internal references.[20] The genomes of patients and healthy donor were used as a template for qPCR detections. Finally, the data were analyzed by using the $2^{-\Delta\Delta Ct}$ method.

Western Blot

The spacer gel (6%) and separation gel (10%) were first prepared according to standard protocols. In the meantime, the protein samples were adjusted to be the same concentrations by using the loading buffer, which was followed with 10 min at 100°C and an immediate ice shock. To detect the low-abundance proteins, a total of 20–40 μg of samples was loaded for each lane. Then, the electrophoresis was run at conditions of 80 V for 40 min and 120 V for 1 h. When the electrophoresis was finished, the semi-dry transferring system was prepared to transfer the protein from the gel into the polyvinylidene fluoride (PVDF) membrane (0.22 μm) at 20 V (40 min). Then, the PVDF membrane was blocked with 5% non-fat milk for 1 h after the brief washing in deionized water, which was followed with incubations of primary antibodies at 4°C overnight. On the next day, the membrane was washed with Tris-buffered saline with Tween 20 (TBST) buffer three times and incubated with secondary antibodies for 1 h at room temperature. At last, the targeted bands were detected and recorded in the machine by adding the enhanced chemiluminescence (ECL) exposure reagent. To detect cytochrome *c* release of mitochondria, the mitochondria were carefully removed from cells for protein extraction.

Immunostaining

Cells were cultured on cover slides to the desired density and fixed in 4% PFA. Then, the slides were blocked by 1% BSA (Sigma) at room

Figure 7. Functional Restoration of CYP4V2$^{-/-}$ RPE Cells Treated with AAV2-CYP4V2

(A) Reduced lipid accumulations in CYP4V2$^{-/-}$ RPE cells upon AAV treatments. (i) Representative images showed decreased LDs in CYP4V2$^{-/-}$ RPE cells stained with BODIPY-493/503 after AAV treatments. Scale bars, 25 μm. (ii) Compared with the untreated group, LDs were significantly decreased in CYP4V2$^{-/-}$ PRE cells upon AAV treatments. A one-way ANOVA and Newman-Keuls were used: *p < 0.05, **p < 0.001, ***p < 0.0001 (mean ± SEM values, n = 4,000 cells). (B) Decreased mtROS in CYP4V2$^{-/-}$ RPE cells upon AAV treatments. (i) Representative images showed decreased mtROS in CYP4V2$^{-/-}$ RPE cells stained with MitoTracker and MitoSOX after AAV treatments. Scale bars, 25 μm. (ii) Compared with the untreated group, mtROS were significantly decreased in CYP4V2$^{-/-}$ PRE cells upon AAV treatments. A one-way ANOVA and Newman-Keuls test were used: *p < 0.05, **p < 0.001, ***p < 0.0001 (mean ± SEM values, n = 3). (C) Recovered functions of mitochondrial respiration in CYP4V2$^{-/-}$ RPE cells upon AAV treatments. The OCR was normalized based on the protein concentration of the cells. wt, CYP4V2^{wt}; +/−, CYP4V2$^{+/-}$; −/−, CYP4V2$^{-/-}$. A one-way ANOVA and Newman-Keuls test were used: ***p < 0.0001 (mean ± SEM values, n = 3). (D) Reduced apoptosis in CYP4V2$^{-/-}$ RPE cells upon AAV treatments. (i) Representative images show a decreased annexin V-positive population in CYP4V2$^{-/-}$ RPE cells upon AAV treatments. (ii) Compared with the untreated group, the annexin V-positive population is significantly decreased in CYP4V2$^{-/-}$ PRE cells. A one-way ANOVA and Newman-Keuls test were used: ***p < 0.0001 (mean ± SEM values, n = 3). (E) Recovered PUFA resistance in CYP4V2$^{-/-}$ RPE cells upon AAV treatments. Compared to the untreated group, significantly decreased cell death in CYP4V2$^{-/-}$ RPE cells treated with AAV upon AA and EPA stimulations is shown. A t test (two-tailed) and paired test were used: *p < 0.05, **p < 0.01, ***p < 0.001; all versus −/− (mean ± SEM values, n = 3). (F) Recovered hydroxyl PUFAs in CYP4V2$^{-/-}$ RPE cells upon AAV treatments. Compared to the untreated group, significantly increase hydroxyl PUFAs were revealed in CYP4V2$^{-/-}$ RPE cells upon AAV treatments. A t test (two-tailed) and paired test were used: *p < 0.05, **p < 0.01, ***p < 0.001; all versus −/− (mean ± SEM values, n = 3). (G) Recovered PUFAs in CYP4V2$^{-/-}$ RPE cells upon AAV treatments. Compared to the untreated group, PUFAs were significantly decreased in CYP4V2$^{-/-}$ RPE cells upon AAV treatments. A t test (two-tailed) and paired test were used: *p < 0.05, **p < 0.01, ***p < 0.001; all versus −/− (mean ± SEM values, n = 3).

temperature for 1 h after treatment with Triton X-100. After washing several times with PBS, primary antibodies were added prior to overnight incubation at 4°C. Finally, an LSM 700 confocal microscope (Carl Zeiss) was utilized to observe the slides after incubation with secondary antibodies.

Germ Layer Differentiation

Confluent PSCs were treated with Accutase and then flushed into clumps with iPSC basal medium. The cell clumps were transferred into the low attached cell culture plate for embryoid body (EB) formation. 7 days late, the EBs were cultured on Geltrex-coated cover slides for a further 14 days. Finally, the differentiated cells were fixed for staining three germ layer markers, including nestin, smooth muscle actin (SMA), and alpha-fetoprotein (AFP).

RPE Differentiation and Characterization

The classic EB-mediated method was used for RPE differentiation.[35] Briefly, PSCs were split and cultured on low-adherent cell culture plates to form EBs, which were cultured on RPE medium for 1 week and transferred onto Geltrex-coated plates to induce cell differentiation. After 4–5 weeks, black cell clumps were collected and seeded on a new Geltrex-coated plate. Mature and pigmented RPE cells were usually obtained 1 month later (these RPE cells were set as P0). For RPE characterization, all PREs were seeded and cultured on cover slides for 1 month to detect protein markers (ZO-1, bestrophin, CRALBP, and RPE65) by immunostaining (these RPE cells were set as P1). To measure the TER of differentiated RPE cells, the cells were seeded on Geltrex-coated transwells at a density of 100,000/cm^2. The TER was recorded once a week four times using the EVOM epithelial voltohmmeter according to its operating instructions. The empty Geltrex-coated transwell containing the medium was set as control. After TER measurement, cells were fixed and scraped for TEM characterization (these RPE cells were set as P1). For the phagocytosis assay, the retinas were collected from 8-week-old rats and cut into small pieces in RPE medium,[74] then co-cultured with the polarized RPE cells.[75] After 2 days of incubation, the RPE cells were flushed three times to remove the retina and dead cells. Then, cells were fixed for staining with anti-rhodopsin (rats) and anti-ZO-1 (humans).[76] Nine RPEs were used for functional studies, including healthy 1-RPE, patient 1-RPE, patient 2-RPE, H9-RPE, H9-CYP4V2$^{+/-}$-RPE, H9-CYP4V2$^{-/-}$-RPE, IMR90-RPE, IMR90-CYP4V2$^{+/-}$- RPE, and IMR90-CYP4V2$^{-/-}$-RPE. All RPEs used for further functional studies were cultured for at least 1 month before treatments or assays, and they were not cultured to the fifth passage, at which point the RPE cells would lose their natural morphology and functions.[77]

Lipid Staining and Fatty Acid Uptake

BODIPY-493/503 (Thermo Fisher Scientific) and BODIPY-C12 (Thermo Fisher Scientific) were utilized to determine lipid accumulation and fatty acid uptake in cells. Cells were cultured to the desired status and washed twice with PBS. Then, BODIPY-493/503 (5 μM) or BODIPY-C12 (5 μM) was added, and the cells were incubated in the dark at 37°C. After 15 min, the dye was removed and the cells washed three times with PBS before being examined. Cells were observed using a confocal microscope. More than 4,000 cells were counted. The images were processed using ImageJ, and the fluorescent signal was collected and quantified for statistical analysis.

Detection of mtROS

MitoSOX Red (Thermo Fisher Scientific) and MitoTracker Green (Thermo Fisher Scientific) were used to label mitochondrial ROS and mitochondria of the targeted cells. Cells were cultured to the desired density and washed twice with PBS. Then, MitoSOX Red (2 μM) and MitoTracker Green (200 nM) were mixed in the PBS. After 15 min of incubation at 37°C, PBS was removed. Cells were washed three times with PBS before being observed. For PSCs, cells were collected and suspended in staining reagents, then analyzed by flow cytometry (BD Biosciences). To normalize the results, the signals of stained PSCs (WT), including the MitoTracker and MitoSOX, were adjusted to the baseline. RPE cells were observed using a confocal microscope. More than 4,000 cells were counted. The images were processed using ImageJ, and the fluorescent signal was collected and quantified for statistical analysis.

RNA Sequencing and Data Analysis

To reduce the genetic variations from different patient samples, total RNA of six cultured parallel PSC controls (H9, H9-CYP4V2$^{+/-}$, H9-CYP4V2$^{-/-}$, IMR90, IMR90-CYP4V2$^{+/-}$, and IMR90-CYP4V2$^{-/-}$) and derived RPE cells (H9-RPE, H9-RPE-CYP4V2$^{+/-}$, H9-RPE-CYP4V2$^{-/-}$, IMR90-RPE, IMR90-RPE-CYP4V2$^{+/-}$, and IMR90-RPE-CYP4V2$^{-/-}$) were sent for RNA sequencing in addition to the donors' iPSCs and derived PRE cells. Then, the raw data were assembled and aligned to human genome hg38 using HISAT2 and Cufflinks to generate fragments per kilobase of transcript per million mapped reads (FPKM). Next, Cuffdiff was used to calculate and identify the differentially expressed genes (FC > 1.5, $p < 0.05$) based on the comparison between *CYP4V2* mutant and WT cells. GSEA is a knowledge-based approach to evaluate the functional relevance of genome-wide expression profiles based on Gene Ontology (GO) biological processes and Kyoto Encyclopedia of Genes and Genomes (KEGG) pathways.[42] It can examine whether a set of pre-defined genes show significant differences between two biological phenotypes or conditions. In this study, we first ranked all of the genes based on the FC of gene expressions between two conditions of CYP4V2^{wt} and CYP4V2^{mt} RPE cells. We assessed the functional relevance of the input genes based on the enrichment analysis by $p < 0.05$ and q value.

Measurement of Mitochondrial Respiration

To evaluate the function of mitochondria, OCR was measured using the Seahorse XF24 flux analyzer (Seahorse). Briefly, RPE cells were seeded in the 24-well Seahorse culture plate at a consistent density and cultured to induce cell polarization. Glutamine, glucose, and sodium pyruvate were then added to the basal medium to prepare a working medium with pH 7.4. Cells were washed three times with

the working medium, and the drugs, including oligomycin (1.5 μM), carbonyl cyanide *p*-trifluoromethoxy-phenylhydrazone (FCCP) (0.5 μM), and rotenone (1 μM), were prepared. When programming was complete, cells were loaded into the Seahorse machine for OCR testing.

Annexin V Assay

The RPE cells were cultured for 4 weeks to stimulate the cell polarization and lipid accumulations. To stain the apoptotic cells, the annexin V/PI working solution was prepared according to the protocol in the kit. Then, the cells were gently washed three times with PBS and digested into single cells by using TrypLE Select enzyme. After centrifugation, approximately 100,000 RPE cells were re-suspended with the annexin V/PI working solution and incubated in the dark for 15 min at room temperature. Then, the staining was stopped by the ice incubation after adding 400 μL of assay buffer, which should be analyzed by using the flow cytometry as soon as possible. CYP4V2^{wt} RPE cells were stained with annexin V and PI individually and used for the compensation of fluorescent signal with a BD FACSCanto II analyzer. Then, unstained CYP4V2^{wt} RPE cells were used as negative controls for gating setup. At last, all of the RPE cells were co-stained with annexin V and PI to record the fluorescence intensity.[78]

GC-MS for Total Cellular Fatty Acids

The classic Ficoll method was utilized to extract the total cellular lipids of the targeted cells.[79] The internal standard was added during the whole process. After esterification, the methyl ester was eluted with *n*-hexane for GC-MS (Agilent Technologies). SCAN and SIM modes were set in the Agilent 7890B GC-MS machine, and the DB-23 capillary column was used to separate the fatty acids. For the GC program, the starting temperature was 50°C (1 min); the temperature was then increased to 175°C (25°C/min) and 190°C (3.5°C/min, 5-min hold). Finally, the temperature was enhanced to 220°C (2°C/min, 11-min hold). The Agilent MassHunter WorkStation quantitative analysis software was used for data analysis. Linear calibration curves for each analyte were generated by plotting the peak area ratio of external/internal standard against the standard concentration at different concentration levels. Analytes were confirmed by comparing the ratio of characteristic fragment ions in the sample and standard. The mol % was used to quantify each fatty acid, and the results were normalized with the WT prior to statistical analysis.[9,31]

LC-MS for Hydroxyl Fatty Acids

The method used for hydroxyl fatty acid testing was modified according to Song et al.'s work.[38] Briefly, cells were re-suspended with 500 μL of methanol containing 0.48 mg of butylated hydroxytoluene (BHT) and mixed with 100 μL of internal standards for ultrasonication on ice, followed by centrifugation at 4°C (12,000 rpm for 10 min). Supernatant was collected and dried in N_2. To remove impurities, samples were eluted with 15% methanol containing 0.005% formic acid and purified by solid-phase extraction (SPE) column. Finally, the hydroxyl fatty acids were eluted with 50 μL of methanol for LC-MS detection (Agilent Technologies). An Agilent Zorbax Eclipse Plus C18 column (2.1 × 100 mm, 1.8 μm) was used with the temperature set to 48°C. Acetonitrile and deionized water were used as a mobile phase. To separate all hydroxyl fatty acids, the flow velocity was set as 0.65 mL/min for 13 min of collection. For GC conditions, multiple reaction monitoring (MRM) in negative ion mode was used.

Fatty Acid Treatment

All polarized RPE cells were treated with fatty acids, including MA, PA, SA, LA, ALA, AA, and EPA (Sigma). The fatty acids were eluted in fatty acid-free BSA, and the final concentration was adjusted to 8 mM. To establish the killing curve, different concentration gradients were used for SFAs (0, 100, and 200μM) and for PUFAs (0, 20, 40, 80, 160, and 200 μM). After 1 week of fatty acid treatment, dead cells were observed and recorded by normal light microscopy. Trypan blue staining was used to identify dead cells that were collected and counted by a cell counter to quantify the percentage of dead cells, using the WT cell as a control. For fatty acid stimulation experiments, AA (40 μM) and EPA (40 μM) were used. RPE cells were treated for 5 days before other functional tests were carried out.

AAV2-CYP4V2 Construction and Gene Therapy

To construct the AAV2-CYP4V2 plasmid, the open reading frame (ORF) of *CYP4V2* was amplified using cDNA of a healthy donor as a template. Then, it was cloned into an AAV2 core vector for *E. coli* transformation. After the verification of Sanger sequencing, the AAV2-CYP4V2 plasmid was sent to a commercial company for virus packaging (BioWit Technologies, China). Three CYP4V2$^{-/-}$ RPE cell lines derived from patient 2, CYP4V2$^{-/-}$ IMR90 and H9, were treated by AAV2 with an MOI of 20,000 using empty AAV2-infected RPE cells as a control. 12 h later, fresh medium was changed and cells were culture for 1 week before the expression confirmation. For further functional studies, AAV2-treated PRE cells were cultured for 1 month to stimulate the cell polarization.

Laboratory Animals

SCID mice were used for teratoma formation in this project. All protocols adhered to the *Guidelines for the Care and Use of Laboratory Animals* prepared by the National Academy of Sciences and published by the National Institutes of Health, and was approved by the Committee on the Use of Live Animals in Teaching and Research at the University of Hong Kong.

IRB Ethics

For human biopsies used in this project, it was necessary to obtain the approval from the Institutional Review Board (IRB) of the University of Hong Kong/Hospital Authority Hong Kong West Cluster (HKU/HA HKW IRB). The IRB reference number is UW 14-557.

Statistical Analysis

Data were analyzed by Prism 5 (GraphPad). Statistical analysis was performed using t tests and ANOVA. Data are presented as mean ± SEM. $p < 0.05$ was considered significant.

SUPPLEMENTAL INFORMATION

Supplemental Information can be found online at https://doi.org/10.1016/j.ymthe.2020.07.024.

AUTHOR CONTRIBUTIONS

Conceptualization, Z.Z. and Q. Lian; Methodology, Z.Z., Q. Lian, B.Y., F.G., P.C., L.Z., W.D., C.L.,W.X., S.H., and H.F.; Investigation, Z.Z. and Q. Lian; Resources, Q. Lian, X.M., Q. Li, Y.L., J.C., and Z.Y.; Manuscript Writing, Z.Z. and Q. Lian; Manuscript Revision, Z.Z., B.Y., and Q. Lian; Supervision and Funding Resource, Q. Lian.

CONFLICTS OF INTEREST

The authors declare no competing interests.

ACKNOWLEDGMENTS

This research was supported in part by the National Natural Science Grant of China (nos. 31571407 and 31270967 to Q. Lian); the Hong Kong Research Grant Council General Research Fund (nos. HKU17113816 and HKU772510M to Q. Lian); the Hong Kong Health and Medical Research Fund (HMRF) (no. 06172956 to Q. Lian); the Guangzhou Women and Children's Medical Centre Grant (no. 5001-4001010); and by The Key Grant from the Science and Technology Foundation of Guangdong Province of China (no. 2015B020225001). The AAV backbone vector was kindly gifted by the Prof. Patrick Aubgourg Laboratory.

REFERENCES

1. Bietti, G. (1937). Uber familiares Vorkommen von "Retinitis punctata albescens" (verbunden mit "Dystrophia marginalis cristalinea corneae"). Glitzen des Glaskorpers und anderen degenerativen Augenveranderungen. Lin. Mbl. Augenh. *99*, 737–745.

2. Hu, D.-N. (1983). Ophthalmic genetics in China. Ophthalmic Paediatr. Genet. *2*, 39–45.

3. Wilson, D.J., Weleber, R.G., Klein, M.L., Welch, R.B., and Green, W.R. (1989). Bietti's crystalline dystrophy. A clinicopathologic correlative study. Arch. Ophthalmol. *107*, 213–221.

4. Halford, S., Liew, G., Mackay, D.S., Sergouniotis, P.I., Holt, R., Broadgate, S., Volpi, E.V., Ocaka, L., Robson, A.G., Holder, G.E., et al. (2014). Detailed phenotypic and genotypic characterization of Bietti crystalline dystrophy. Ophthalmology *121*, 1174–1184.

5. Kojima, H., Otani, A., Ogino, K., Nakagawa, S., Makiyama, Y., Kurimoto, M., Guo, C., and Yoshimura, N. (2012). Outer retinal circular structures in patients with Bietti crystalline retinopathy. Br. J. Ophthalmol. *96*, 390–393.

6. Li, A., Jiao, X., Munier, F.L., Schorderet, D.F., Yao, W., Iwata, F., Hayakawa, M., Kanai, A., Shy Chen, M., Alan Lewis, R., et al. (2004). Bietti crystalline corneoretinal dystrophy is caused by mutations in the novel gene *CYP4V2*. Am. J. Hum. Genet. *74*, 817–826.

7. Nakano, M., Kelly, E.J., and Rettie, A.E. (2009). Expression and characterization of CYP4V2 as a fatty acid ω-hydroxylase. Drug Metab. Dispos. *37*, 2119–2122.

8. Nakano, M., Kelly, E.J., Wiek, C., Hanenberg, H., and Rettie, A.E. (2012). CYP4V2 in Bietti's crystalline dystrophy: ocular localization, metabolism of ω-3-polyunsaturated fatty acids, and functional deficit of the p.H331P variant. Mol. Pharmacol. *82*, 679–686.

9. Lai, T.Y., Chu, K.O., Chan, K.P., Ng, T.K., Yam, G.H., Lam, D.S., and Pang, C.P. (2010). Alterations in serum fatty acid concentrations and desaturase activities in Bietti crystalline dystrophy unaffected by *CYP4V2* genotypes. Invest. Ophthalmol. Vis. Sci. *51*, 1092–1097.

10. Lockhart, C.M., Nakano, M., Rettie, A.E., and Kelly, E.J. (2014). Generation and characterization of a murine model of Bietti crystalline dystrophy. Invest. Ophthalmol. Vis. Sci. *55*, 5572–5581.

11. Zhang, Z., Zhang, Y., Gao, F., Han, S., Cheah, K.S., Tse, H.F., and Lian, Q. (2017). CRISPR/Cas9 genome-editing system in human stem cells: current status and future prospects. Mol. Ther. Nucleic Acids *9*, 230–241.

12. Lamba, D.A., Gust, J., and Reh, T.A. (2009). Transplantation of human embryonic stem cell-derived photoreceptors restores some visual function in *Crx*-deficient mice. Cell Stem Cell *4*, 73–79.

13. Schwartz, S.D., Regillo, C.D., Lam, B.L., Eliott, D., Rosenfeld, P.J., Gregori, N.Z., Hubschman, J.P., Davis, J.L., Heilwell, G., Spirn, M., et al. (2015). Human embryonic stem cell-derived retinal pigment epithelium in patients with age-related macular degeneration and Stargardt's macular dystrophy: follow-up of two open-label phase 1/2 studies. Lancet *385*, 509–516.

14. Hata, M., Ikeda, H.O., Iwai, S., Iida, Y., Gotoh, N., Asaka, I., Ikeda, K., Isobe, Y., Hori, A., Nakagawa, S., et al. (2018). Reduction of lipid accumulation rescues Bietti's crystalline dystrophy phenotypes. Proc. Natl. Acad. Sci. USA *115*, 3936–3941.

15. Mengda, L., Xiaobei, Y., Ting, H., Xiaowei, S., and Genlin, L. (2015). Changes of serum lipids in patients with Bietti crystalline dystrophy. Chin. J. Exp. Ophthalmol. *33*, 47–50.

16. Naso, M.F., Tomkowicz, B., Perry, W.L., 3rd, and Strohl, W.R. (2017). Adeno-associated virus (AAV) as a vector for gene therapy. BioDrugs *31*, 317–334.

17. Zarbin, M. (2016). Cell-based therapy for degenerative retinal disease. Trends Mol. Med. *22*, 115–134.

18. Jiao, X., Li, A., Jin, Z.B., Wang, X., Iannaccone, A., Traboulsi, E.I., Gorin, M.B., Simonelli, F., and Hejtmancik, J.F. (2017). Identification and population history of CYP4V2 mutations in patients with Bietti crystalline corneoretinal dystrophy. Eur. J. Hum. Genet. *25*, 461–471.

19. Meng, X.H., He, Y., Zhao, T.T., Li, S.Y., Liu, Y., and Yin, Z.Q. (2019). Novel mutations in *CYP4V2* in Bietti corneoretinal crystalline dystrophy: next-generation sequencing technology and genotype-phenotype correlations. Mol. Vis. *25*, 654–662.

20. Astuti, G.D., Sun, V., Bauwens, M., Zobor, D., Leroy, B.P., Omar, A., Jurklies, B., Lopez, I., Ren, H., Yazar, V., et al. (2015). Novel insights into the molecular pathogenesis of *CYP4V2*-associated Bietti's retinal dystrophy. Mol. Genet. Genomic Med. *3*, 14–29.

21. Meng, X.H., Guo, H., Xu, H.W., Li, Q.Y., Jin, X., Bai, Y., Li, S.Y., and Yin, Z.Q. (2014). Identification of novel *CYP4V2* gene mutations in 92 Chinese families with Bietti's crystalline corneoretinal dystrophy. Mol. Vis. *20*, 1806–1814.

22. Yin, X., Yang, L., Chen, N., Cui, H., Zhao, L., Feng, L., Li, A., Zhang, H., Ma, Z., and Li, G. (2016). Identification of *CYP4V2* mutation in 36 Chinese families with Bietti crystalline corneoretinal dystrophy. Exp. Eye Res. *146*, 154–162.

23. Shan, M., Dong, B., Zhao, X., Wang, J., Li, G., Yang, Y., and Li, Y. (2005). Novel mutations in the CYP4V2 gene associated with Bietti crystalline corneoretinal dystrophy. Mol. Vis. *11*, 738–743.

24. Biasini, M., Bienert, S., Waterhouse, A., Arnold, K., Studer, G., Schmidt, T., Kiefer, F., Gallo Cassarino, T., Bertoni, M., Bordoli, L., and Schwede, T. (2014). SWISS-MODEL: modelling protein tertiary and quaternary structure using evolutionary information. Nucleic Acids Res. *42*, W252-8.

25. Huang, X., Chou, B.-K., Mali, P., Ye, Z., Dowey, S.N., and Cheng, L. (2010). Human IPS cells generated from adult peripheral blood cells and purified $CD34^+$ cells by a non-integrating plasmid. Blood *116*, 1589.

26. Su, R.-J., Baylink, D.J., Neises, A., Kiroyan, J.B., Meng, X., Payne, K.J., Tschudy-Seney, B., Duan, Y., Appleby, N., Kearns-Jonker, M., et al. (2013). Efficient generation of integration-free iPS cells from human adult peripheral blood using BCL-XL together with Yamanaka factors. PLoS ONE *8*, e64496.

27. Ran, F.A., Hsu, P.D., Wright, J., Agarwala, V., Scott, D.A., and Zhang, F. (2013). Genome engineering using the CRISPR-Cas9 system. Nat. Protoc. *8*, 2281–2308.

28. Meaney, M.J. (2001). Maternal care, gene expression, and the transmission of individual differences in stress reactivity across generations. Annu. Rev. Neurosci. *24*, 1161–1192.

29. El-Brolosy, M.A., and Stainier, D.Y.R. (2017). Genetic compensation: a phenomenon in search of mechanisms. PLoS Genet. *13*, e1006780.

30. Qiu, B., and Simon, M.C. (2016). BODIPY 493/503 staining of neutral lipid droplets for microscopy and quantification by flow cytometry. Biol. Protoc. *6*, e1912.

31. Jüttner, F. (2001). Liberation of 5,8,11,14,17-eicosapentaenoic acid and other polyunsaturated fatty acids from lipids as a grazer defense reaction in epilithic diatom biofilms. J. Phycol. *37*, 744–755.

32. Cardona, F., Túnez, I., Tasset, I., Montilla, P., Collantes, E., and Tinahones, F.J. (2008). Fat overload aggravates oxidative stress in patients with the metabolic syndrome. Eur. J. Clin. Invest. *38*, 510–515.

33. Schaffer, J.E. (2016). Lipotoxicity: many roads to cell dysfunction and cell death: introduction to a thematic review series. J. Lipid Res. *57*, 1327–1328.

34. Halliwell, B. (1991). Reactive oxygen species in living systems: source, biochemistry, and role in human disease. Am. J. Med. *91* (3C), 14S–22S.

35. Idelson, M., Alper, R., Obolensky, A., Ben-Shushan, E., Hemo, I., Yachimovich-Cohen, N., Khaner, H., Smith, Y., Wiser, O., Gropp, M., et al. (2009). Directed differentiation of human embryonic stem cells into functional retinal pigment epithelium cells. Cell Stem Cell *5*, 396–408.

36. Liang, G., and Zhang, Y. (2013). Genetic and epigenetic variations in iPSCs: potential causes and implications for application. Cell Stem Cell *13*, 149–159.

37. Lin, J., Nishiguchi, K.M., Nakamura, M., Dryja, T.P., Berson, E.L., and Miyake, Y. (2005). Recessive mutations in the *CYP4V2* gene in East Asian and Middle Eastern patients with Bietti crystalline corneoretinal dystrophy. J. Med. Genet. *42*, e38.

38. Song, J., Liu, X., Wu, J., Meehan, M.J., Blevitt, J.M., Dorrestein, P.C., and Milla, M.E. (2013). A highly efficient, high-throughput lipidomics platform for the quantitative detection of eicosanoids in human whole blood. Anal. Biochem. *433*, 181–188.

39. Houten, S.M., and Wanders, R.J. (2010). A general introduction to the biochemistry of mitochondrial fatty acid β-oxidation. J. Inherit. Metab. Dis. *33*, 469–477.

40. Wakil, S.J., and Abu-Elheiga, L.A. (2009). Fatty acid metabolism: target for metabolic syndrome. J. Lipid Res. *50* (*Suppl*), S138–S143.

41. Hegarty, B.D., Cooney, G.J., Kraegen, E.W., and Furler, S.M. (2002). Increased efficiency of fatty acid uptake contributes to lipid accumulation in skeletal muscle of high fat-fed insulin-resistant rats. Diabetes *51*, 1477–1484.

42. Subramanian, A., Tamayo, P., Mootha, V.K., Mukherjee, S., Ebert, B.L., Gillette, M.A., Paulovich, A., Pomeroy, S.L., Golub, T.R., Lander, E.S., and Mesirov, J.P. (2005). Gene set enrichment analysis: a knowledge-based approach for interpreting genome-wide expression profiles. Proc. Natl. Acad. Sci. USA *102*, 15545–15550.

43. Weigel, A.L., Handa, J.T., and Hjelmeland, L.M. (2002). Microarray analysis of H_2O_2-, HNE-, or tBH-treated ARPE-19 cells. Free Radic. Biol. Med. *33*, 1419–1432.

44. Lelliott, C., and Vidal-Puig, A.J. (2004). Lipotoxicity, an imbalance between lipogenesis de novo and fatty acid oxidation. Int. J. Obes. Relat. Metab. Disord. *28* (*Suppl 4*), S22–S28.

45. Assies, J., Mocking, R.J., Lok, A., Ruhé, H.G., Pouwer, F., and Schene, A.H. (2014). Effects of oxidative stress on fatty acid- and one-carbon-metabolism in psychiatric and cardiovascular disease comorbidity. Acta Psychiatr. Scand. *130*, 163–180.

46. Nowak, J.Z. (2013). Oxidative stress, polyunsaturated fatty acids-derived oxidation products and bisretinoids as potential inducers of CNS diseases: focus on age-related macular degeneration. Pharmacol. Rep. *65*, 288–304.

47. Brand, M.D., and Nicholls, D.G. (2011). Assessing mitochondrial dysfunction in cells. Biochem. J. *435*, 297–312.

48. Miller, E. (2004). Apoptosis measurement by annexin V staining. Methods Mol. Med. *88*, 191–202.

49. Sawai, H., and Domae, N. (2011). Discrimination between primary necrosis and apoptosis by necrostatin-1 in annexin V-positive/propidium iodide-negative cells. Biochem. Biophys. Res. Commun. *411*, 569–573.

50. Yang, H., and Li, X. (2012). The role of fatty acid metabolism and lipotoxicity in pancreatic β-cell injury: identification of potential therapeutic targets. Acta Pharm. Sin. B *2*, 396–402.

51. Yu, J., and Zhang, L. (2008). PUMA, a potent killer with or without p53. Oncogene *27* (*Suppl 1*), S71–S83.

52. Qin, J.-Z., Stennett, L., Bacon, P., Bodner, B., Hendrix, M.J., Seftor, R.E., Seftor, E.A., Margaryan, N.V., Pollock, P.M., Curtis, A., et al. (2004). p53-independent NOXA induction overcomes apoptotic resistance of malignant melanomas. Mol. Cancer Ther. *3*, 895–902.

53. Gao, Y., Liang, W., Hu, X., Zhang, W., Stetler, R.A., Vosler, P., Cao, G., and Chen, J. (2010). Neuroprotection against hypoxic-ischemic brain injury by inhibiting the apoptotic protease activating factor-1 pathway. Stroke *41*, 166–172.

54. Cai, J., Yang, J., and Jones, D.P. (1998). Mitochondrial control of apoptosis: the role of cytochrome *c*. Biochim. Biophys. Acta *1366*, 139–149.

55. Uauy, R., Hoffman, D.R., Peirano, P., Birch, D.G., and Birch, E.E. (2001). Essential fatty acids in visual and brain development. Lipids *36*, 885–895.

56. Serini, S., Piccioni, E., Merendino, N., and Calviello, G. (2009). Dietary polyunsaturated fatty acids as inducers of apoptosis: implications for cancer. Apoptosis *14*, 135–152.

57. Ulloth, J.E., Casiano, C.A., and De Leon, M. (2003). Palmitic and stearic fatty acids induce caspase-dependent and -independent cell death in nerve growth factor differentiated PC12 cells. J. Neurochem. *84*, 655–668.

58. Moloudizargari, M., Mortaz, E., Asghari, M.H., Adcock, I.M., Redegeld, F.A., and Garssen, J. (2018). Effects of the polyunsaturated fatty acids, EPA and DHA, on hematological malignancies: a systematic review. Oncotarget *9*, 11858–11875.

59. Merkle, F.T., and Eggan, K. (2013). Modeling human disease with pluripotent stem cells: from genome association to function. Cell Stem Cell *12*, 656–668.

60. Nagy, K., and Tiuca, I.-D. (2017). Importance of fatty acids in physiopathology of human body. In Fatty Acids (IntechOpen), pp. 3–22.

61. Gülcan, H.G., Alvarez, R.A., Maude, M.B., and Anderson, R.E. (1993). Lipids of human retina, retinal pigment epithelium, and Bruch's membrane/choroid: comparison of macular and peripheral regions. Invest. Ophthalmol. Vis. Sci. *34*, 3187–3193.

62. Reddy, J.K., and Hashimoto, T. (2001). Peroxisomal β-oxidation and peroxisome proliferator-activated receptor α: an adaptive metabolic system. Annu. Rev. Nutr. *21*, 193–230.

63. Hardwick, J.P. (2008). Cytochrome P450 omega hydroxylase (CYP4) function in fatty acid metabolism and metabolic diseases. Biochem. Pharmacol. *75*, 2263–2275.

64. Cazanave, S.C., and Gores, G.J. (2010). Mechanisms and clinical implications of hepatocyte lipoapoptosis. Clin. Lipidol. *5*, 71–85.

65. Christen, W.G., Schaumberg, D.A., Glynn, R.J., and Buring, J.E. (2011). Dietary ω-3 fatty acid and fish intake and incident age-related macular degeneration in women. Arch. Ophthalmol. *129*, 921–929.

66. Tanito, M., and Anderson, R. (2009). Dual roles of polyunsaturated fatty acids in retinal physiology and pathophysiology associated with retinal degeneration. Clin. Lipidol. *4*, 821–827.

67. Hauck, A.K., and Bernlohr, D.A. (2016). Oxidative stress and lipotoxicity. J. Lipid Res. *57*, 1976–1986.

68. Mao, H., Seo, S.J., Biswal, M.R., Li, H., Conners, M., Nandyala, A., Jones, K., Le, Y.Z., and Lewin, A.S. (2014). Mitochondrial oxidative stress in the retinal pigment epithelium leads to localized retinal degeneration. Invest. Ophthalmol. Vis. Sci. *55*, 4613–4627.

69. Orrenius, S., Gogvadze, V., and Zhivotovsky, B. (2007). Mitochondrial oxidative stress: implications for cell death. Annu. Rev. Pharmacol. Toxicol. *47*, 143–183.

70. Kannan, K., and Jain, S.K. (2000). Oxidative stress and apoptosis. Pathophysiology *7*, 153–163.

71. Abdelmagid, S.A., Clarke, S.E., Nielsen, D.E., Badawi, A., El-Sohemy, A., Mutch, D.M., and Ma, D.W. (2015). Comprehensive profiling of plasma fatty acid concentrations in young healthy Canadian adults. PLoS ONE *10*, e0116195.

72. Wakil, S.J., Stoops, J.K., and Joshi, V.C. (1983). Fatty acid synthesis and its regulation. Annu. Rev. Biochem. *52*, 537–579.

73. Listenberger, L.L., Han, X., Lewis, S.E., Cases, S., Farese, R.V., Jr., Ory, D.S., and Schaffer, J.E. (2003). Triglyceride accumulation protects against fatty acid-induced lipotoxicity. Proc. Natl. Acad. Sci. USA *100*, 3077–3082.

74. Johnson, T.V., and Martin, K.R. (2008). Development and characterization of an adult retinal explant organotypic tissue culture system as an in vitro intraocular stem cell transplantation model. Invest. Ophthalmol. Vis. Sci. *49*, 3503–3512.

75. Subrizi, A., Hiidenmaa, H., Ilmarinen, T., Nymark, S., Dubruel, P., Uusitalo, H., Yliperttula, M., Urtti, A., and Skottman, H. (2012). Generation of hESC-derived retinal pigment epithelium on biopolymer coated polyimide membranes. Biomaterials *33*, 8047–8054.

76. Wu, W., Zeng, Y., Li, Z., Li, Q., Xu, H., and Yin, Z.Q. (2016). Features specific to retinal pigment epithelium cells derived from three-dimensional human embryonic stem cell cultures—a new donor for cell therapy. Oncotarget *7*, 22819–22833.

77. Croze, R.H., Buchholz, D.E., Radeke, M.J., Thi, W.J., Hu, Q., Coffey, P.J., and Clegg, D.O. (2014). ROCK inhibition extends passage of pluripotent stem cell-derived retinal pigmented epithelium. Stem Cells Transl. Med. *3*, 1066–1078.

78. Huang, H., Li, H., Shi, K., Wang, L., Zhang, X., and Zhu, X. (2018). TREK-TRAAK two-pore domain potassium channels protect human retinal pigment epithelium cells from oxidative stress. Int. J. Mol. Med. *42*, 2584–2594.

79. Folch, J., Lees, M., and Sloane Stanley, G.H. (1957). A simple method for the isolation and purification of total lipides from animal tissues. J. Biol. Chem. *226*, 497–509.